Redox Biology 88 (2025) 103908

Contents lists available at ScienceDirect

Redox Biology

journal homepage: www.elsevier.com/locate/redox

Oxidation of hemoglobin to ferryl hemoglobin contributes to remodeling of the artery wall in abdominal aortic aneurysm

Yuchao Ding [a,b,c,1], László Potor [a,b,1], Éva Katona [d], Péter Sótonyi [e], Ágnes Szappanos [f,g], Gergő Péter Gyurok [e], Gábor Méhes [h], Zoltán Hendrik [b,c,i], Attila Fintha [j], Péter Attila Gergely [h], Zoltán Benyó [k,l], Zsolt Combi [a,c], Katalin Éva Sikura [b,m], Lívia Beke [h], Norbert Nemeth [n], Szabo Balazs [n], Ibolya Fürtös [a], Gergő Kalló [o], Éva Csősz [o], Szilárd Póliska [p], Andreas Patsalos [q], E Sebastian Debus [r], László Nagy [p,q,*], György Balla [b,m,**], József Balla [a,b,***]

[a] Division of Nephrology, Department of Internal Medicine, Faculty of Medicine, University of Debrecen, Hungary
[b] HUN-REN-UD Vascular Pathophysiology Research Group, University of Debrecen, Hungary
[c] Kálmán Laki Doctoral School, University of Debrecen, Debrecen, Hungary
[d] Department of Laboratory Medicine, Faculty of Medicine, University of Debrecen, Debrecen, Hungary
[e] Heart and Vascular Center, Department of Vascular Surgery and Endovascular Surgery, Semmelweis University, Budapest, Hungary
[f] Heart and Vascular Centre, Semmelweis University, Budapest, Hungary
[g] Department of Rheumatology and Clinical Immunology, Semmelweis University, Budapest, Hungary
[h] Department of Pathology, Faculty of Medicine, University of Debrecen, Hungary
[i] Institute of Forensic Medicine, Faculty of Medicine, University of Debrecen, Hungary
[j] Department of Pathology and Experimental Cancer Research, Semmelweis University, Budapest, Hungary
[k] Institute of Translational Medicine, Semmelweis University, Budapest, Hungary
[l] HUN-REN-SU Cerebrovascular and Neurocognitive Diseases Research Group, Budapest, Hungary
[m] Department of Pediatrics, Faculty of Medicine, University of Debrecen, Hungary
[n] Department of Operative Techniques and Surgical Research, Faculty of Medicine, University of Debrecen, Debrecen, Hungary
[o] Proteomics Core Facility, Department of Biochemistry and Molecular Biology, Faculty of Medicine, University of Debrecen, Debrecen, Hungary
[p] Department of Biochemistry and Molecular Biology, Faculty of Medicine, University of Debrecen, Debrecen, Hungary
[q] Departments of Medicine and Physiology, Pharmacology and Therapeutics, and Biomedical Engineering, Johns Hopkins University School of Medicine and Institute for Fundamental Biomedical Research, All Children's Hospital, St. Petersburg, Florida, 33701, USA
[r] Department of Vascular Medicine, Vascular Surgery, Angiology, Endovascular Therapy, University of Hamburg-Eppendorf, Hamburg, Germany

ARTICLE INFO

Keywords:
Abdominal aortic aneurysm
Hemoglobin oxidation
Neutrophil granulocytes
Macrophages
CD163

ABSTRACT

Abdominal aortic aneurysm (AAA) with potentially fatal outcomes affects cardiovascular health via inflammation-related abnormalities. We revealed the presence of the oxidized hemoglobin (Hb), ferrylHb in the circulation in patients diagnosed with ruptured AAA. The aim of our study was to identify the source of oxidation of Hb in human hemorrhaged AAA and in an angiotensin II provoked AAA model in mice leading to generation of ferrylHb and to describe its fate in the pathophysiology. We demonstrate that two electron oxidations of Hb leading to the formation of ferrylHb with the characteristics of oxidation of βCys93, αCys104, and βCys112 residues is the terminal product of the interaction of neutrophils and macrophages with Hb in the hemorrhaged AAA. This oxidized Hb, ferrylHb is taken up by neutrophils and macrophages via CD163 mediated endocytosis with subsequent activations including peptidylarginine deiminase 4 (PAD4) driven NETosis, liberation of elastase, myeloperoxidase and subsequent degradation of extracellular matrix. AAA exhibits increased expression of CD163 in macrophages and neutrophils revealed to be inducible by ferrylHb involving PAD4 signaling. RNA-seq analysis demonstrated that human ruptured AAA has a unique transcriptomic profile, different from healthy

* Corresponding author. Departments of Medicine and Physiology, Pharmacology and Therapeutics, and Biomedical Engineering, Johns Hopkins University School of Medicine and Institute for Fundamental Biomedical Research, All Children's Hospital, St. Petersburg, Florida, 33701, USA.
** Corresponding author. Department of Pediatrics, Faculty of Medicine, University of Debrecen, Hungary.
*** Corresponding author. Division of Nephrology, Department of Internal Medicine, Faculty of Medicine, University of Debrecen, Nagyerdei krt. 98., Pf. 19., 4032 Debrecen, Hungary.
E-mail address: balla@belklinika.com (J. Balla).
[1] The authors share the first authorship.

https://doi.org/10.1016/j.redox.2025.103908
Received 11 September 2025; Received in revised form 21 October 2025; Accepted 27 October 2025
Available online 28 October 2025

aorta, with a 43 % overlap in the differential gene expressions of human macrophages exposed to ferrylHb. Among these 884 genes, we found inflammatory-, angiogenesis-, and tissue remodeling gene clusters. These data suggest that oxidation of Hb to ferryl state and the interactions of neutrophils and macrophages with ferrylHb within aortic wall contribute to AAA progression.

1. Introduction

Abdominal aortic aneurysm (AAA) with potentially fatal outcomes affects cardiovascular health via inflammation-related abnormalities [1–4], and neutrophil granulocytes and macrophages are implicated in the pathogenesis [5–8]. Neutrophils were demonstrated to infiltrate vessel walls during the progression of AAA [9,10] and contribute to the loss of vessel integrity [5,6,11]. Depletion of circulating neutrophils was shown to inhibit AAA development in mice in an elastase perfusion experimental model [5]. The retardation of neutrophil infiltration of artery walls in L-selectin-deficient mice inhibited AAA formation [6]. Neutrophils in the aorta are particularly sensitive to extracellular activators, among them to inducers for generating reactive oxygen species, to mechanical stretching, and to neurohormonal factors [12]. In parallel to neutrophils, macrophages also accumulate within the aortic wall during AAA progression, where they contribute to extracellular matrix degradation and amplify inflammatory responses, further promoting vessel wall weakening [13].

Neutrophils have the capability to generate extracellular reticular structures known as neutrophil extracellular traps (NETs), comprising histones, granule proteins, and depolymerized genomic DNA through a process called NETosis [14]. Neutrophil proteases, elastase and proteinase-3 were revealed to promote AAA via extracellular trap release [15,16]. NETs exacerbate inflammation and induce endothelial- and vascular smooth muscle cell death [17], thus closely linking them to AAA. Inhibition of NET formation reduces neutrophil infiltration in the arterial wall [18], and mitigates AAA formation [19].

Intramural hemorrhage is characteristic of the progression of AAA [9,20]. It was shown that neutrophils and macrophages readily oxidize hemoglobin (Hb) [21,22] and globin radicals are formed when metHb reacts with peroxides [23]. The reaction is rapid (within seconds) and results in metHb oxidation at two sites; heme is oxidized to the ferryl form, and a free radical is formed on the globin chain [23,24]. The spectral fingerprints of the transient ferryl-Hb can be captured by a spectrophotometric method [25]. This method has been applied to quantify the oxidative states of heme-iron in Hb within complicated atherosclerotic plaques of carotid arteries showing that 55 % of the total Hb is ferryl-Hb, 39 % is metHb, and 1.4 % is ferroHb [22]. Redox cycling of human metHb by peroxides has been revealed to yield persistent ferryl iron and protein-based radicals [26].

While studies have highlighted a notable protective effect of reducing neutrophil infiltration and NET formation on AAA, the causal role of the interaction between neutrophils and Hb in aortic aneurysm progression remains uncertain. In this study, we uncovered significant abnormalities in Hb-, neutrophil- and macrophage markers both in AAA patients and in angiotensin II (AngII)-induced AAA in apolipoprotein E-deficient ($ApoE^{-/-}$) mice models, and elucidated their causal relationship. Our findings indicate that Hb and ferrylHb exacerbate AAA progression by enhancing neutrophil activation, inducing cell death, and promoting NET formation within the aortic wall. By raising a novel mouse monoclonal antibody against human ferrylHb and developing an ELSA method for measurement of ferrylHb antigen concentrations we detected elevated circulating ferrylHb levels in patients diagnosed with ruptured AAA.

2. Methods

2.1. Study approval

The participation of patients undergoing open aneurysm surgeries was in accordance with the research protocol approved by the Hungarian National Center for Public Health and Pharmacy (No. 164482) and the Regional and Institutional Committee on Scientific and Research Ethics of Semmelweis University (No. 7891/2012). In addition, the operation of the aortic aneurysm biobank was approved by the Hungarian National Center for Public Health and Pharmacy (No. 9882–8/2022) and the Regional and Institutional Committee on Scientific and Research Ethics of Semmelweis University (No. 111/2022). In compliance with the EüM decree, the human studies were conducted in accordance with applicable laws and the Helsinki Declaration of the World Federation of Physicians. All patients or their proxies provided written informed consent before specimen collection. The presence of an aortic aneurysm was documented before surgery using echocardiography or computed tomography angiography/magnetic resonance imaging. Expert vascular specialist established clinical diagnoses before surgery. The surgical indication for infrarenal AAA was 5.5 cm in men and 5.0 cm in women, which was not ruptured and showed no signs of infection. Aortic samples were conserved, stored, and used for scientific research in accordance with European Union legislation. We adhere to the provisions of the Basic Law of Hungary and current legislation regarding personal rights, the protection of personal health data, and copyright protection during research.

An aortic aneurysm biobank was established for the purpose of examining AAA. The thrombus filling the lumen of the affected vessel from the patient's aortic wall samples, as well as blood, saliva, urine and anal smear are stored in the biobank. Patient demographic findings, clinical data and laboratory parameters are recorded in a database developed for this purpose. For all patients included in the study, aortic wall samples undergo histological analysis. The processing of these histological specimens is performed by cardiovascular expert pathologists.

Healthy aortic tissue samples were obtained from deceased organ donors without aneurysms or other vascular diseases within 4–6 h after organ donation. Sampling of donors is in accordance with international and national legislation and the principles of national multi-organ donation. The study was approved by the Regional and Institutional Committee on Scientific and Research Ethics of Semmelweis University (license number: 257/2018.). Donor consent is not available, as the analysis of vascular tissue from brain-dead donors during multi-organ donation was done anonymously. In accordance with the General Data Protection Regulation of the European Union, the anonymous data of the donors were prospectively collected from the donor's electronic health information system.

Detailed information regarding the patients, and deceased organ donors is listed in Tables 1 and 2. Neutrophils and macrophages from healthy volunteers were isolated from whole blood (Regional Research Ethical Committee, Project No.: 3853–2013 and 4699–2016) (Table 3).

Animal experiments performed in this study were approved by the Scientific and Research Ethics Committee of the Scientific Council of Health of the Hungarian Government under the registration number 1/2021/DEMÁB. The Institutional and National Guidelines for the care and use of animals were followed. C57BL/6 $ApoE^{-/-}$ mice were maintained at the University of Debrecen under specific pathogen-free conditions in accordance with guidelines from the Institutional Ethical

Table 1
Clinical characteristics of patients with abdominal aortic aneurysm.

Parameters	Data
Sampling period	From January 2022 to January 2025.
Total sample number	Out of a total of 42 samples, 40 were utilized for serum measurement, 10 for histological analysis, and 10 were allocated for spectrophotometric analysis, proteomic analysis, biochemical examinations, molecular biology studies, and RNA sequencing.
Gender	33 males (33/42, 78.6 %); 9 Females (9/42, 21.4 %).
Age	59–80 years (average: 69.3 years, SD: 5.4 years).
Localization	Suprarenal (1/42, 2.4 %); Infrarenal (25/42, 59.5 %); Suprarenal and infrarenal (2/42, 4.8 %); Juxta renal (11/42, 26.1 %); Thoracal (1/42, 2.4 %); Iliac (2/42, 4.8 %).
Aneurysm morphology	Fusiform (34/42, 80.9 %); Saccular (6/42, 14.3 %); Dual (2/42, 4.8 %).
Symptoms	Asymptomatic (33/42, 78.6 %); Symptomatic (8/42, 19.0 %); Uncertain (1/42, 2.4 %).
Maximal axial diameter (mm)	41–82 mm (average: 60.1 mm, SD: 11.2 mm).
Progression (mm/year)	2–19 mm/year (average: 7.0 mm/year, SD: 3.9 mm/year; 21/42, 50 %); Primary detected before the surgery (21/42, 50 %).
Comorbidities and conditions of patients	Hypertension (33/42, 78.6 %); Ischemic heart disease (6/42, 14.3 %); Type 2 diabetes mellitus (NIDDM; 6/42, 14.3 %); Stroke (ischemic and hemorrhagic; 5/42, 11.9 %); Hyperlipidemia (8/42, 19.0 %); Myocardial infarction (AMI; 8/42, 19.0 %); COPD (9/42, 21.4 %); Hypothyroidism (3/42, 7.1 %); Heart surgery-CABG (0/42, 0 %); Bronchial asthma (1/42, 2.4 %); Glaucoma (2/42, 4.8 %); Cancer (12/42, 28.6 %).
Intensity of inflammation in abdominal aortic aneurysm according to histological analysis	None (1/42, 2.4 %); Mild (2/42, 4.8 %); Moderate (4/42, 9.5 %); Serious (6/42, 14.2 %); Tertiary lymphoid tissue (28/42, 66.7 %); No data (1/42, 2.4 %).
Most frequent medications	Antiplatelet (33/42, 78.6 %); Antacids (7/42, 16.6 %); Beta-blocker (19/42, 45.2 %); Diuretics (8/42, 19.0 %); Allopurinol (6/42, 14.3 %); Calcium channel blocker (10/42, 23.8 %); ACE inhibitor or ATII receptor antagonists (12/42, 28.6 %); Statins (15/42, 35.7 %); Alpha 1-receptor blocker (6/42, 14.3 %); Levothyroxine (8/42, 19.0 %); Anticholinergic (4/42, 9.5 %).

FerrylHb, ferryl hemoglobin; SD, standard deviation; NIDDM, noninsulin-dependent diabetes mellitus; COPD, chronic obstructive pulmonary disease; CABG, coronary artery bypass surgery; ACE inhibitor, angiotensin-converting-enzyme inhibitor; ATII receptor, angiotensin II receptor.

Table 2
Clinical characteristics of healthy individuals.

Parameters	Data
Sampling period	From 2022 to 2025
Total sample number	Out of a total of 31 samples, 26 were utilized for serum measurement, 5 (from organ donors) for histological analysis, spectrophotometric analysis, proteomic analysis, biochemical examinations, molecular biology studies, and RNA sequencing.

Committee.

2.2. Measurement of ferryl hemoglobin level in serum

After the development and characterization of a novel anti-ferrylHb monoclonal antibody (ferrylHb specific mouse monoclonal antibody: anti-ferrylHb mAb [22]), we established an in-house sandwich ELSA method for measurement of ferrylHb antigen concentrations. The epitope of the antibody located to the LLVVYPWTQR sequence at positions 32–41 of the beta subunit and exposed only in oxidized Hb [22]. Flat-bottomed 96-well high-binding ELISA plates (EB, Thermo Fischer Scientific Oy Vantaa, Finland) were coated with unlabeled anti-ferrylHb mAb (10 μg/ml, 0.1 ml/well in 0.2 M $NaHCO_3$, pH 9.6) and incubated overnight at 4 °C. Plates were blocked with 0.15 ml/well assay buffer (0.5 % BSA 0.5 M NaCl and 0.05 % Tween 20 in PBS, pH: 7.2) for 1 h at room temperature. After blocking, 0.1 ml/well standard or serum samples, diluted 1:2500 in assay buffer, were added and plates were incubated for 1 h at room temperature. In the next step, captured ferrylHb was incubated with 0.1 ml/well of HRPO-labeled anti-ferrylHb mAb for 1 h at room temperature and developed using 0.1 ml/well of 3,3′,5,5′-Tetramethyl-benzidine (TMB, One Component HRP Microwell Substrate, Diarect Ag, Freiburg, Germany). After 15 min at room temperature, the reaction was stopped by adding 0.05 ml/well 2 M H_2SO_4, and the absorbance was read at 450 nm using a Labsystems iEMS MF microplate reader (Labsystems Oy, Helsinki, Finland). Between all incubation steps, wells were washed three times with PBS containing 0.05 % Tween 20 (0.3 ml/well). A diluted series of ferrylHb in the range of 2.5–100 μg/l was used in parallel to create calibration curves. The within-run coefficient of variation of the assay was 4.1 %, 5.9 %, and 7.1 % for samples with 189 μg/ml, 98 μg/ml, and 22 μg/ml ferrylHb, respectively.

Table 3
Data of healthy blood donor volunteers (Isolation of neutrophils and macrophages from whole blood).

Parameters	Data
Sampling period	From September 2023 to August 2025
Total volunteer number	8
Total sample number	21
Gender	8 Males (100 %)
Age	25–62 Years (average: 41.1 years, SD: 11.5 years)

2.3. Mouse abdominal aortic aneurysms model induction

Eight-to ten-week-old male $ApoE^{-/-}$ mice were randomly assigned to either the AngII infusion group or the saline infusion group. Only male mice were used due to the potential influence of female sex hormones on AngII and the male predominance in human aortic hematoma. Mice were fed either an high-fat diet (HFD) containing 18 % protein, 12.6 % carbohydrate, 15 % fat, and 1.25 % cholesterol (Sniff Spezialdiäten GmbH, DE-59494, Soest, Germany) or a standard diet (STD) for 12 weeks. During the last 4 weeks, they were subcutaneously infused with 1000 ng/min/kg AngII (Sigma-Aldrich Corp., St. Louis, MO) or saline through an osmotic minipump (Model 2004; ALZA Scientific Products, Mountain View, CA).

At the end of the 12-week study period, mice were euthanized via intraperitoneal injection of a mixture of ketamine (80 mg/kg) and xylazine (5 mg/kg). The aorta of each mouse was exposed and rinsed with cold saline, and the peri-aortic tissues were removed. The aorta was then excised, further cleaned, and rinsed with cold saline to remove any residual blood from the lumen. Segments of the abdominal aorta were processed for AAA evaluation and tissue analysis or were snap-frozen for protein analysis. Macroscopic pictures of the arteries were taken with a Nikon D3200 camera (Nikon Corp.; Minato, Tokyo, Japan).

2.4. Abdominal ultrasonography in mice

In vivo ultrasonography of the abdominal aortas was performed using the Vevo 3100 (MX550D) ultrasound system with a 32 MHz linear transducer (FUJIFILM VisualSonics, Inc., Toronto, Canada). Mice were

anesthetized with 1 %–2 % isoflurane. After shaving the abdominal hair, mice were transferred to and fixed on the imaging stage in a supine position. Ultrasound transmission gel was then applied to the abdominal skin. Long-axis ultrasound scans of the suprarenal aorta were conducted from the aortic hiatus to the left renal artery. Images of the abdominal aorta were captured at mid-systole. The maximal internal diameters of the aorta were measured by two independent investigators in a blinded manner.

2.5. Blood pressure and heart rate measurements

Systolic blood pressure and heart rate were measured using a CODA noninvasive blood pressure system (tail-cuff method, Kent Scientific Corporation) before and after pump implantation. Briefly, mice were placed in a holder on an Animal Warming Platform. An occlusion cuff and a volume pressure recording (VPR) cuff were placed near the base of the tail and connected to the CODA Controller. Ten measurement cycles were performed, with accepted cycles automatically displayed in a spreadsheet format within the CODA application. Data were then processed in Microsoft Excel to calculate the average and standard deviation.

2.6. Classification of aneurysm severity

The severity of aortic aneurysm was classified according to our previously reported modification of the classification system described by Daugherty and colleagues [27,28]: Stage I, normal aorta; Stage II, aortic aneurysm without hemorrhage; Stage III, aortic aneurysm with hemorrhage; and Stage IV, ruptured aorta. Aneurysmal tissue was evaluated by three independent observers who were blinded to the experimental groups. In the case of a discrepancy, the observers discussed the case and reached a consensus on the classification.

2.7. Histology

Tissue sections (human and mouse samples) of 4 μm thickness from representative formalin-fixed paraffin-embedded tissues were used for serial Hematoxylin-eosin (H&E), Naphthol AS-D (NASD) chloroacetate esterase staining, Verhoeff-Van Gieson (EVG) staining, Masson's trichrome staining, and special immunohistochemistry (IHC) staining. Deparaffinization, antigen retrieval, and staining for myeloperoxidase (MPO), Hb, ferrylHb, and cluster of differentiation 163 (CD163) antibodies were performed according to the manufacturer's instructions. Anti-MPO antibody (Thermo Scientific, RB373A) was used at a dilution of 1:1000 for 1 h; anti-Hb antibody (Abcam, ab92492, clone: EPR3608) at a dilution of 1:500 for 1 h; mouse monoclonal anti-human ferrylHb antibody (developed by our group) at a dilution of 1:100 for 1 h; and the CD163 primary antibody (Cat. No. 16646-1-AP, Proteintech) was incubated at a 1:500 dilution for 1 h. After rinsing with PBS, the slides were incubated with the MACH 2 Rabbit HRP-Polymer (cat. No.: RP520H, Biocare, Concord, CA, USA) for 30 min, followed by chromogen staining using the DAB Chromogen Kit and a subsequent H_2O rinse. Slides were then counterstained with Mayer's hematoxylin for 1 min and rinsed with tap water for 10 min. Finally, slides were dehydrated through graded alcohols to xylene and mounted. For digital documentation, slides were scanned with a Mirax Midi scanner (3D Histech, Budapest, Hungary).

Elastin degradation was quantified using a grading system based on EVG staining, which evaluates the integrity, waviness, and fragmentation of elastic fibers. The grading was performed as follows [29]: Grade 1 (normal), Intact, organized elastin fibers with a wavy appearance; Grade 2, Visible breaks, partial loss of waviness, and some fragmentation of elastic fibers; Grade 3, Significant fragmentation, with ≥50 % loss of elastin signal or structural integrity; Grade 4, Severe disruption, most or all elastic fibers broken or absent, often accompanied by increased collagen and disorganization. Three independent observers performed the grading. To minimize potential artifacts due to tissue processing, all aortic samples were handled consistently using standardized fixation, dehydration, and embedding protocols. Sections were cut at uniform thickness and stained in parallel to ensure comparability.

2.8. Immunofluorescent staining

Cells were fixed in 3.7 % formaldehyde for 15 min and then permeabilized with 0.3 % Triton X-100 for 15 min. The scavenger receptor CD163 or MPO were stained using a rabbit anti-CD163 primary antibody (Novus Biologicals, NB110-40686) or rabbit anti-MPO primary antibody (Thermo Scientific, RB373A), followed by an Alexa Fluor 488 F (ab')2 fragment of goat anti-rabbit IgG (H + L) secondary antibody (Cat. No. A11070, Thermo Fisher Scientific Inc., Waltham, MA, USA). FerrylHb was stained using a mouse monoclonal primary antibody (developed by our group), followed by an Alexa Fluor 568 F (ab')2 fragment of goat anti-mouse IgG (H + L) secondary antibody (Cat. No. A11004, Thermo Fisher Scientific Inc., Waltham, MA, USA). Nuclei were stained with Hoechst 33,258. The CD163, MPO and ferrylHb primary antibodies were incubated at a 1:500 dilution for 1 h at room temperature. All secondary antibodies were used at a 1:500 dilution for 1 h at room temperature.

For tissue samples (human and mouse, $n = 5$/group) were labeled with mouse anti-human ferrylHb antibody (dilution of 1:1000 for 2 h) and stained with Alexa Fluor 488 F (ab')2 fragment of goat anti-mouse IgG (H + L) at a dilution of 1:1000 for 2 h (Cat no. A11070, Thermo Fisher Scientific Inc., Waltham, MA U.S.A.), and labeled with rabbit anti-human CD163 antibody (Abcam, ab182422) at a dilution of 1:400 for 2 h, and stained with Alexa Fluor 647 of goat anti-rabbit IgG (H + L) at a dilution of 1:1000 for 2 h (Cat no. A21244, Thermo Fisher Scientific Inc., Waltham, MA U.S.A.), or labeled with either anti-MPO (Thermo Scientific, RB373A) or anti-CD68 antibodies (Invitrogen, PA5-78996) at a dilution of 1:500 for 1 h, and stained with Alexa Fluor 568 of goat anti-rabbit IgG (H + L) at a dilution of 1:500 for 1 h (Invitrogen, A11011).

In other cases, human samples ($n = 5$/group) were labeled with mouse anti-human ferrylHb antibody (dilution of 1:1000 for 2 h) and stained with Alexa Fluor 488 F (ab')2 fragment of goat anti-mouse IgG (H + L) at a dilution of 1:1000 for 2 h (Cat no. A11070, Thermo Fisher Scientific Inc., Waltham, MA U.S.A.), and labeled with rabbit anti-human MPO antibody (Cat. No. RB373A, Thermo Fisher Scientific Inc., Waltham, MA, USA) at a dilution of 1:1000 for 2 h or with rabbit anti-human carboxypeptidase M (CPM) antibody (ab150405 clone: EPR8052; Abcam Plc, Cambridge, United Kingdom) at a dilution of 1:200 for 1 h, and stained with Alexa Fluor 647 of goat anti-rabbit IgG (H + L) at a dilution of 1:1000 for 2 h (Cat no. A21244, Thermo Fisher Scientific Inc., Waltham, MA U.S.A.).

2.9. Western blot

Human healthy arteries ($n = 4$) and AAA ($n = 5$) were homogenized in liquid nitrogen. The samples were then solubilized in protein lysis buffer (10 mmol/l Tris-HCl, 5 mmol/l EDTA, 150 mmol/l NaCl, pH 7.2), 1 % Triton X-100, 0.5 % Nonidet P-40, and protease inhibitors (Complete Mini, F. Hoffmann-La Roche Ltd., Basel, Switzerland). 50 μg of protein from each sample were loaded onto 10 % SDS-polyacrylamide gels. After electrophoresis, proteins were transferred to a nitrocellulose membrane (Amersham Biosciences Corp., Piscataway, NJ, USA). The blot was incubated overnight with HRP-conjugated goat anti-human Hb antibody (Cat. No. ab19362-1, Abcam Plc., Cambridge, UK) at a dilution of 1:15,000 or with mouse anti-human ferrylHb antibody labeled with HRP (developed by our group) at a dilution of 1:1000, followed by HRP-conjugated secondary antibody. Antigen-antibody complexes were detected using chemiluminescence according to the manufacturer's instructions (GE Healthcare Life Sciences, Piscataway, NJ, USA).

10 mm sections of aneurysm tissue from mice ($n = 3$/group) were taken and placed in protein lysis buffer. The samples were then sonicated three times for 10 s on ice, followed by centrifugation at 12.000*g*

for 15 min at 4 °C. Eighteen micrograms of protein from each sample were loaded onto 10 % SDS-polyacrylamide gels. The Hb protein was detected by incubating the membrane overnight with goat anti-human Hb antibody (Cat. No. ab19362-1, Abcam Plc., Cambridge, UK) at a dilution of 1:5000.

Human neutrophils were treated with 10 μmol/l Hb or 10 μmol/l ferrylHb for 24 h, followed by solubilization in protein lysis buffer. 20 μl of the supernatant samples, after protein isolation, were applied to 10 % SDS-PAGE gels. The MPO protein was detected by incubating the membrane overnight with rabbit anti-human MPO antibody (Thermo, RB373A) at a dilution of 1:15,000, followed by incubation with HRP-conjugated anti-rabbit secondary antibody (Cell Signaling, 7074S) at a dilution of 1:15,000 for 1 h.

Human neutrophils were treated with 10 μmol/l Hb or 10 μmol/l PMA for 16 h. After treatment, the cells were solubilized in protein lysis buffer. 20 μg of total protein were applied to 10 % SDS-PAGE gels. The Hb protein was detected by incubating the membrane overnight with rabbit anti-human Hb antibody (Cat. No. ab19362-1, Abcam Plc., Cambridge, UK) at a dilution of 1:5000.

Human neutrophils were treated with 5 μmol/l ferrylHb or 5 μmol/l GSK484 for 16 h. After treatment, 37.5 μl of total supernatant samples were applied to 10 % SDS-PAGE gels. The CD163 protein was detected by incubating the membrane overnight with rabbit anti-human CD163 antibody (Cat. No. 16646-1-AP, Proteintech) at a dilution of 1:500. The MPO protein was detected by incubating the membrane overnight with rabbit anti-human MPO antibody (Cat. No. RB373A, Thermo) at a dilution of 1:500.

Human macrophages were treated with 5 μmol/l ferrylHb or 5 μmol/l GSK484 for 16 h. After treatment, 20 μg of total proteins were applied to 10 % SDS-PAGE gels. The CD163 protein was detected by incubating the membrane overnight with rabbit anti-human CD163 antibody (Cat. No. 16646-1-AP, Proteintech) at a dilution of 1:500. Uncropped raw images of all blots were included as Source Data.

2.10. Immunoprecipitation

Human healthy arteries ($n = 4$) and AAA ($n = 5$) were homogenized in liquid nitrogen. Then, the samples were solubilized in protein lysis buffer (10 mM Tris-HCl, 5 mM EDTA, and 150 mM NaCl, pH 7.2), 1 % Triton X-100, 0.5 % Nonidet P-40, and protease inhibitors (Complete Mini; F. Hoffmann-La Roche Ltd.). Pierce Protein A/GTM magnetic agarose beads (40 μl, Cat. No. 78609; Thermo Scientific, Waltham, MA) were added to a 1.5 ml microcentrifuge tube. A total of 460 μl of binding/wash buffer (10 mM phosphate buffer [pH 7.4], 150 mM NaCl) was added to the beads. The tube was placed into a magnetic stand to collect the beads against the side of the tube. The supernatant was removed and discarded. Binding/wash buffer (0.5 ml) was added to the tube and gently mixed for 1 min. The beads were collected with the magnetic stand, and the supernatant was removed and discarded.

Anti-human ferrylHb antibody at a 10-fold higher concentration than that used for Western blotting was added to a total volume of binding/wash buffer of 500 μl. The antibody-bead mixture was incubated for 4 h at 4 °C by gentle mixing on a suitable shaker. The tube was placed into a magnetic stand to collect the beads against the side of the tube, and the supernatant was removed and discarded. Binding/wash buffer (0.5 ml) was added to the tube and gently mixed for 1 min. The washing step was repeated twice. Fifteen microliters of tissue lysate was added with 450 μl of binding/wash buffer to a 1.5 ml microcentrifuge tube. The lysate-bead/antibody conjugate mixture was incubated at 4 °C under rotary agitation for 16 h. The beads were washed three times with binding/wash buffer containing a 1:20 volume of protease inhibitor. The tube was placed into a magnetic stand to collect the beads against the side of the tube, and the supernatant was removed and discarded. One hundred microliters of elution buffer (0.1 M glycine, pH 2.0–3.0) was added to the tube and incubated for 10 min at room temperature with occasional mixing. The beads were collected with a magnetic stand, and the supernatant was then removed and saved. To neutralize the low pH, 100 μl of neutralization buffer (1 M Tris-HCl, pH 7.5) was added for each 100 μl of eluate. Western blot analysis was performed using anti-human ferrylHb antibody for the detection of ferrylHb in abdominal aorta samples.

2.11. Hemoglobin separation and purification

OxyHb (Fe^{2+}) was prepared as described before [30]. Hb was isolated from fresh blood drawn from healthy volunteers and purified using ion-exchange chromatography on a DEAE Sepharose CL-6B column. The isolation process yielded 98–99 % oxyHb, with 1–2 % of Hb underwent oxidation. Aliquots were snap-frozen in liquid nitrogen and stored at −70 °C. The purity of the Hb preparation was assessed by silver staining. Hb concentrations were calculated as described by Winterbourn [31]. In this study, Hb concentration was always expressed as heme concentration.

2.12. Analysis of various redox states of hemoglobin

Human healthy arteries and AAA tissues ($n = 5$/group) were placed in saline. The samples were then sonicated three times for 10 s on ice using an Ultrasonic Cell Disrupter (Virtis Virsonic 323,410), followed by centrifugation at 12.000*g* for 15 min at 4 °C. The supernatants were analyzed using a spectrophotometer (Beckman Coulter Inc., Brea, CA, USA). The following equations were used to measure the contents of oxyHb, metHb, and ferrylHb in the aneurysm tissues [32].

$$[\text{OxyHb}] = -75.78OD_{560} + 103.16OD_{576} - 38.39OD_{630}$$

$$[\text{MetHb}] = -26.09OD_{560} + 12.48OD_{576} - 280.70OD_{630}$$

$$[\text{FerrylHb}] = 132.60OD_{560} - 74.10OD_{576} - 68.33OD_{630}$$

The processing method for mouse aneurysm samples was the same as described above.

After 16 h of treatment with PMA or Hb, neutrophils were collected. The concentrations of different redox states of Hb were determined by analyzing the visible spectra.

2.13. Determination of total heme content

Heme measurements in the healthy aorta and AAA tissue samples were performed as previously described by our study and by Huy et al. [33,34].

2.14. LC-MS/MS analysis

Mouse aorta lysates (STD + Saline, $n = 2$; HFD + Saline, $n = 2$; STD + AngII, $n = 2$; HFD + Saline, $n = 2$), human healthy aortic tissue lysates ($n = 5$) and human aneurysm lysates with rupture ($n = 5$) were subjected to in-solution trypsin digestion. Proteins were denatured with 6 M urea (Bio-Rad, Hercules, CA, USA) for 30 min; thereafter, reduced with 10 mM dithiothreitol (Bio-Rad, Hercules, CA, USA) at 56 °C for 60 min and further alkylated with 20 mM iodoacetamide (Bio-Rad, Hercules, CA, USA) in the dark for 45 min at room temperature. Before trypsin digestion, samples were diluted with 25 mM ammonium bicarbonate (Sigma-Aldrich, St. Louis, MO, USA) to decrease the urea concentration to 1 M. Trypsin digestion was performed at 37 °C overnight by adding MS-grade modified trypsin (Sciex, Framingham, MA, USA) in 1:25 enzyme to protein ratio. The digested proteins were dried in speed-vac and dissolved in 1 % formic acid. The samples were desalted with C18 PierceTips (ThermoFisher Scientific, Waltham, MA, USA), dried, and re-dissolved in 1 % formic acid before mass spectrometry analyses.

The LC-MS/MS analysis of trypsin-digested samples was carried out on Easy nLC 1200 ultra-performance liquid chromatography coupled to the Orbitrap Fusion mass spectrometer (Thermo Scientific, Waltham,

MA, USA). The peptide mixtures were desalted on an ACQUITY UPLC Symmetry C18 trap column (20 mm × 180 μm, 5 μm particle size, 100 Å pore size, Waters, Milford, MA, USA), followed by separation on an Acclaim PepMap RSLC column (75 μm × 250 mm, 2 μm particle size, 100 Å pore size, Thermo Scientific, Waltham, MA, USA). The chromatographic separation was done using a 180-min-long gradient, 5 % solvent B over 5 min, followed by a rise to 10 % of solvent B over 5 min, and then to 35 % solvent B over 120 min. Thereafter, solvent B was increased to 50 % over 15 min and then to 85 % over 5 min, followed by a 10-min rise to 85 % of solvent B, after which the system returned to 5 % solvent B in 1 min for a 19-min hold-on. Solvent A was 0.1 % formic acid in LC water (Merck, Darmstadt, Germany); solvent B was 95 % acetonitrile (Merck, Darmstadt, Germany) containing 0.1 % formic acid. The flow rate was set to 400 nl/min.

Data-dependent acquisition experiments were carried out by selecting the top 14 ions from each survey scan (scan range: 350–1600 *m/z*, Orbitrap analyzer resolution: 60,000, AGC target: 4.0e5, acquired in profile mode) for MS/MS analyses. HCD fragmentation was performed with 35 % normalized collision energy and MS/MS spectra were registered in the linear ion trap (AGC target: 1.0e6, acquired in centroid mode). Dynamic exclusion was enabled during the cycles (45 s exclusion time).

2.15. Data processing and analysis

Protein identification was done with MaxQuant 2.0.1 software [35] searching against the Human SwissProt database for human aortic aneurysm samples (release: 2022.01, 20,394 sequence entries) and Mouse SwissProt database (release: 2022.02, 17,082 sequence entries) for mouse aortic aneurysm samples along with the contaminants database provided by the MaxQuant software. Cys oxidation, trioxidation, and carbamidomethylation along with Met oxidation and N-terminal acetylation were set as variable modifications. A maximum of two missed cleavage sites were allowed. The results were imported into the Scaffold 5.0.1 software (Proteome Software, Inc.). Proteins were accepted with at least 2 identified peptides using a 1 % protein false discovery rate and 95 % peptide probability thresholds.

Human Hb was visualized using CAVER Analyst 2.0 software with RCSB PDB entry 1BUW, while mouse Hb was visualized using RCSB PDB entry 3HRW.

2.16. Separation of human blood-derived monocytes and treatment of macrophages

The human macrophages used were derived from blood monocytes collected from healthy donors. Monocytes were separated using density-gradient centrifugation with Histopaque-1077 and differentiated into macrophages over 6 days in Dulbecco's Modified Eagle Medium (DMEM) containing 15 % FBS and 50 ng/ml M-CSF. After 6 days, macrophages were treated with 10 μM of ferrylHb for 8 h at 37 °C in 0 % FBS-containing DMEM [22].

2.17. Isolation of neutrophils from whole blood

Twenty milliliters of anticoagulated blood were collected from healthy volunteers into a 50 ml conical plastic tube and diluted with 20 ml of 0.9 % saline. The blood was then carefully layered on 10 ml of polysucrose and sodium diatrizoate solution (Histopaque®-1077; Product No: 10,771) and centrifuged at 400 g for 40 min at 24 °C. Following centrifugation, the plasma and the layer containing mononuclear cells were discarded. The polymorphonuclear leukocytes, which had some erythrocyte contamination, were collected into a new tube. The cells were resuspended in <5 ml of sterile distilled water for 25 s and then the tonicity was promptly restored by adding an equal volume of 1.8 % sterile saline. The cells were then washed with 0.9 % saline and centrifuged at 500 g for 5 min at 24 °C. Finally, the cells were resuspended in 500 μl of 10 % DMEM with high glucose.

2.18. Neutrophils treated with hemoglobin or ferryl hemoglobin

Neutrophils were isolated, resuspended in DMEM, and seeded into 24-well plates (500 μl/well). The cells were then treated with Hb (10 μmol/l) or ferrylHb (10 μmol/l). Following treatment, the 24-well plates were incubated at 37 °C in a 5 % CO_2 humidified atmosphere for specified durations (4, 8, 16, and 24 h). At each time point, cells were collected and photographed using a Leica DMC 4500 microscope.

To monitor Hb oxidation, neutrophils were stimulated with PMA (10 μg/ml; Product No: P1585) followed by treatment with 10 μmol/l Hb for a total of 16 h.

Human neutrophils were treated with 5 μmol/l ferrylHb or 5 μmol/l GSK484 (ab223598, Abcam) for 16 h.

2.19. Polymorphonuclear leukocyte elastase assay

Polymorphonuclear leukocyte (PMN) elastase was quantified using a Human PMN-Elastase ELISA kit (Affymetrix eBioscience) [36]. Briefly, 10 μl of each sample was added to a microwell plate along with 90 μl of Sample Dilution Buffer and incubated at room temperature for 1 h. After washing, the samples were incubated with 150 μl of HRP-conjugate at room temperature for 1 h. Following another wash, 200 μl of TMB Substrate Solution was added to each well and incubated at room temperature for 30 min in the dark. The reaction was stopped by adding 50 μl of Stop Solution to each well. Absorbance was measured at 450 nm using a microplate reader (PMT 49984, Biotek Synergy HT). Concentrations were expressed as ng/ml.

2.20. RNA-sequencing

To obtain global transcriptome data, high-throughput mRNA sequencing was performed on samples from various groups: Hb and ferrylHb-stimulated human neutrophils ($n = 5$), aortic aneurysm tissues from patients ($n = 4$), healthy aorta samples from organ donors ($n = 5$), and AAA tissues from ApoE$^{-/-}$ mice ($n = 5$/group). Total RNA was extracted from these samples, quantified, and assessed for quality using the Agilent BioAnalyzer with the Eukaryotic Total RNA Nano Kit (Agilent Technologies, Santa Clara, CA, USA), following the manufacturer's protocol. Sequencing was conducted using the Illumina Sequencing Platform (Illumina, San Diego, CA, USA). Due to the high degradation of RNA samples, a ribosomal RNA (rRNA) depletion method was employed to remove rRNA species. The NEBNext ® rRNA Depletion Kit (Human/Mouse/Rat) (New England BioLabs) was utilized for this purpose. For RNA-Seq library preparation, 200 ng of total RNA was used with the NEBNext® Ultra II RNA Sample Preparation Kit for Illumina (New England BioLabs, Ipswich, MA, USA) according to the manufacturer's instructions. Briefly, poly-A-tailed RNAs were purified using oligodT-conjugated magnetic beads. The purified RNAs were fragmented by heating at 94 °C for 15 min. First-strand cDNA synthesis was carried out using random primers, followed by second-strand cDNA synthesis to produce double-stranded cDNA. Following end repair and adapter ligation, the adapter-ligated fragments were amplified through enrichment polymerase chain reaction (PCR) to generate the sequencing libraries. Sequencing was performed on the Illumina NextSeq 500 instrument (Illumina) using single-end 75-cycle sequencing.

2.21. Analysis of RNA-Sequencing data

Raw sequencing data (FASTQ) were aligned to the human or mouse reference genome version (GRCh37) using the HISAT2 algorithm, generating BAM files. Downstream analysis was performed using iDEP 2.01 software (http://ge-lab.org/idep/). BAM files were imported into iDEP 2.01 and DESeq2 algorithm was used for normalization. To identify differentially expressed genes between untreated and ferrylHb-

stimulated conditions, or between aortic aneurysms and healthy aorta, DESeq2 test was applied. ANOVA with Tukey post hoc test was applied to four groups of aorta samples from ApoE$^{-/-}$ mice. Heatmaps and dot plots were drawn using GraphPad Prism 10 (GraphPad Prism Software Inc., La Jolla, CA, USA) or automatically generated by iDEP 2.01. Lists of differentially expressed genes were analyzed using the gene ontology (GO) Enrichment Analysis function in iDEP 2.01. GOs with fold enrichment $\geq$2 and *P*-value <0.05 were selected and results were presented according to their -log10 *P*-value. The bar graph was automatically generated using the iDEP 2.01.

2.22. Statistical

All statistical analyses were conducted using GraphPad Prism 10 (GraphPad Software Inc., La Jolla, CA, USA). Data are presented as mean ± standard error of the mean (SEM), except for mouse blood pressure, heart rate, and the percent survival chart. The normality of the data was assessed using the Shapiro-Wilk test, and the homogeneity of variances was evaluated using Levene's test. For data sets that met the criteria for normality and equal variances, Student's t-test or one-way ANOVA followed by Bonferroni post hoc tests were applied, as indicated in the figure legends. The survival curve was analyzed using the Log-rank and Gehan-Breslow-Wilcoxon tests. The correlation between ferrylHb and heme content was assessed using Pearson's correlation analysis. Statistical significance was determined at a *P*-value of <0.05.

3. Results

3.1. Circulating ferryl hemoglobin in patients with ruptured abdominal aortic aneurysms

We developed a monoclonal antibody-based enzyme-linked immunosorbent assay using anti-ferrylHb monoclonal antibody [22] specific for ferrylHb to measure ferrylHb levels in the serum of patients diagnosed with ruptured AAA and healthy volunteers. Blood samples were collected from 40 patients undergoing open vascular surgery and 26 healthy donors. As shown in Fig. 1A, the mean serum ferrylHb concentration in patients with AAA was significantly elevated (320.12 ± 339.26 μg/ml) compared to healthy individuals (122.36 ± 106.53 μg/ml), with a 2.6-fold increase in ferrylHb concentration in patients ($P < 0.01$). These surprising findings suggest a strong correlation between ferrylHb levels and AAA rupture and prompted us to investigate the source and potential role of ferrylHb in AAA pathophysiology.

3.2. Ferryl hemoglobin accumulates in human abdominal aortic aneurysms associated with hemorrhage and is taken up by neutrophils and macrophages

To examine Hb oxidation and ferrylHb accumulation in AAA, we collected human aneurysmal tissues from ten patients who underwent open AAA repair surgery and healthy aortic tissue samples from five deceased organ donors for analysis (Fig. 1B). The conditions and comorbidities that occurred, as well as medications, are shown in Table 1. As expected, the abdominal aortas from AAA exhibit partial hemorrhage compared to healthy arterial tissues. IHC with anti-ferrylHb antibodies [22] revealed oxidized Hb accumulation both intracellular and extracellular localizations in the aneurysmal arterial wall (Fig. 1C). No ferrylHb was detected in healthy aortas.

Further histopathological analysis revealed extensive disruption of the aortic architecture, characterized by the accumulation of cells with dense and irregular nuclear contours characteristic of granulocytes. These cells were positive for NASD chloroacetate esterase, a granulocyte marker, and MPO [37,38] (Fig. 1C), indicating neutrophil infiltration of the arterial wall that primarily localized around the site of adventitia in the hemorrhagic regions of the AAA. IHC staining for CD163 revealed a high number of CD163-positive cells in the AAA group compared to the healthy controls (Fig. 1C). Additionally, double staining for ferrylHb and MPO confirmed ferrylHb uptake by neutrophils, suggesting a link between Hb oxidation and neutrophil-mediated inflammation in AAA. Double immunofluorescence staining further confirmed the colocalization of ferrylHb with CPM, suggesting that not only neutrophils but also macrophages are involved in the uptake of oxidized Hb, and may contribute to the inflammatory response in AAA (Fig. 1D and Supplemental Fig. 1). Double immunofluorescence staining confirmed robust colocalization of ferrylHb with CD163 (Fig. 1E). Quantitatively, the colocalization rate of ferrylHb with CD163 was 72.37 % ± 3.88 % in neutrophils (MPO-positive cells), whereas the ferrylHb and CD163 colocalization rate was 78.92 % ± 5.89 % in macrophages (CD68-posivive cells) (Fig. 1F). Our study demonstrates significant colocalization of ferrylHb with neutrophils and macrophages, indicating that both leukocytes actively participate in the uptake of oxidized Hb within AAA lesions.

3.3. Oxidation of hemoglobin to the ferryl state followed by oxidative modification of globin chains and liberation of heme moieties occurs in cases of hemorrhaged abdominal aortic aneurysm

Oxidation of Hb and generation of the ferryl form is marked by the formation of cross-linked Hb, a hallmark of ferrylHb [22]. To confirm the presence of ferrylHb in human AAA tissues, we performed Western blot analysis on AAA and healthy abdominal artery tissues. As shown in Fig. 2A, Hb dimers and tetramers (only one of five AAA patients showed a tetramer) accumulated in AAA samples (upper panel), which indicates globin radical formation and covalent crosslinking of globin chains [39]. The presence of ferrylHb in AAA samples was also confirmed by immunoprecipitation (Fig. 2A, lower panel). Spectral analysis [22,25] of AAA tissues revealed significant Hb oxidation compared to controls (Fig. 2B). In ferroHb, as a control, the absorption spectra exhibited two peaks at 542 and 577 nm, which were diminished in AAA samples, indicating the oxidation of Hb. Subsequently, we determined ferrylHb concentrations of oxidized Hb in the same aortic samples using the method described by Alayash [25]. The results from these assays indicate that the ferrylHb levels were significantly elevated in AAA tissues, while ferrylHb was almost undetectable in healthy controls.

Furthermore, Hb oxidation can lead to the release of the heme group from the globin chain, resulting in the formation of non-Hb-bound (free) heme. To investigate this, total heme concentrations were measured in AAA samples showing significantly higher levels of heme (78.29 ± 23.27 μmol/mg protein) compared to healthy controls (7.67 ± 5.86 μmol/mg protein) (Fig. 2C). These findings suggest that oxidation of Hb, generation of ferrylHb, and release of heme moieties are key characteristics of AAA pathophysiology.

Multiple lines of evidence indicate that βCys93 is a critical residue for free radical-induced oxidation of Hb [40–42]. Mass spectrometry was thus employed to identify oxidative modifications of cysteine residues within the Hb molecules in AAA tissues. This analysis confirmed oxidation at βCys93, with additional oxidative modifications identified at βCys112 and αCys104 (Fig. 2D and Proteomics Data 1) [43].

3.4. Hemoglobin oxidation to ferryl hemoglobin is characteristic of angiotensin II-induced abdominal aortic aneurysms in apolipoprotein E-deficient mice

In order to explore further the mechanistic aspects of our findings we employed a mouse model of aortic aneurysm. ApoE$^{-/-}$ mice were fed either a STD or a HFD for 12 weeks, followed by subcutaneous infusion of saline or 1000 ng/kg/min AngII for 28 days to induce AAA (Fig. 3A). The progression of AAA was monitored by measuring the diameter of the abdominal aorta using ultrasonography at 0, 7, 14, and 28 days of AngII infusion (Supplemental Fig. 2A). AngII infusion led to dilation of abdominal aorta in mice, and it was more pronounced in mice on HFD

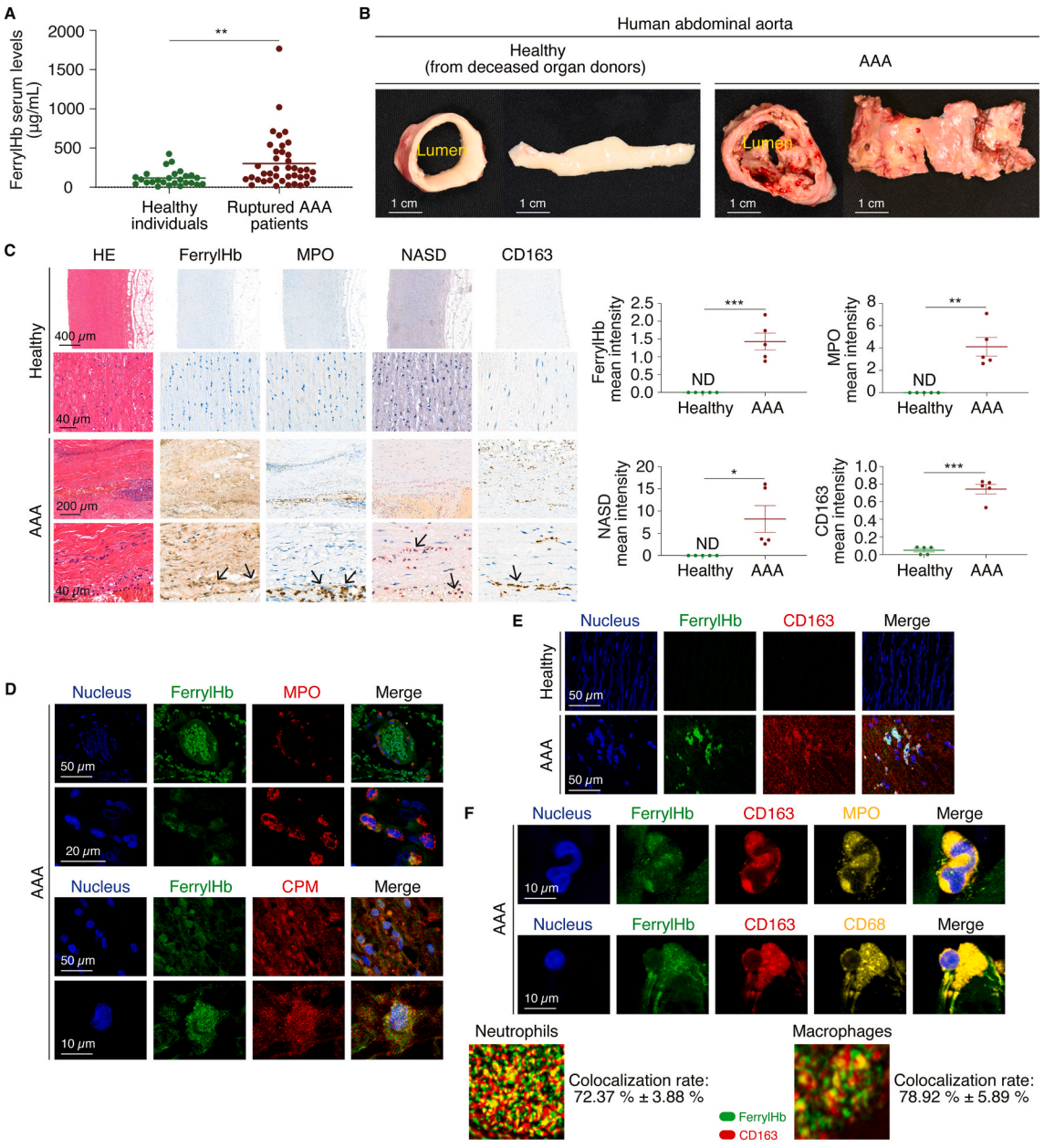

Fig. 1. Circulating ferryl hemoglobin is detected in the blood of patients diagnosed with ruptured abdominal aortic aneurysms, and accumulation of ferryl hemoglobin-positive neutrophils and macrophages in human hemorrhaged aortic aneurysm.

(**A**) We developed an enzyme-linked immunosorbent assay utilizing monoclonal antibodies against human ferryl hemoglobin (ferrylHb) to measure the concentration of ferrylHb in the serum of patients who were diagnosed with ruptured abdominal aortic aneurysm (AAA) and underwent open vascular surgery as well as in healthy volunteers. Results are shown as mean values. Statistical significance was determined using an unpaired *t*-test: $^{**}P < 0.01$ ($n = 26$/healthy donors; $n = 40$/AAA patients). (**B**) Macroscopic views of a hemorrhaged abdominal aorta with an AAA and a healthy aorta harvested from deceased organ donors are shown. (**C**) Hematoxylin-eosin (H&E), ferrylHb immunohistochemical (IHC), myeloperoxidase (MPO), naphthol AS-D chloroacetate esterase (NASD), and CD163 of abdominal aorta tissues are shown ($n = 5$). Quantitative analysis of ferrylHb, MPO, NASD, and CD163 staining of tissue sections was performed using ImageJ software ($n = 5$). $^{*}P < 0.05$; $^{**}P < 0.01$; $^{***}P < 0.001$ (unpaired *t*-test). ND, not detectable. (**D**) Images from the hemorrhagic AAA sections were stained with Hoechst 33,258 to visualize DNA (blue), an anti-ferrylHb antibody coupled with Alexa Fluor 488 to identify ferrylHb (green), and either anti-MPO or anti-carboxypeptidase M (CPM) antibodies conjugated with Alexa Fluor 647 to detect MPO or CPM, respectively (red). (**E** and **F**) Images from the healthy aorta sections and the hemorrhagic AAA sections were stained with Hoechst 33,258 to visualize DNA (blue), an anti-ferrylHb antibody coupled with Alexa Fluor 488 to identify ferrylHb (green), an anti-CD163 antibody coupled with Alexa Fluor 647 to identify CD163 (red), and either anti-MPO or anti-CD68 antibodies conjugated with Alexa Fluor 568 to detect MPO or CD68, respectively (yellow). All images were captured using a Leica TCS SP8 gated STED-CW nanoscopic system and subsequently deconvolved with Huygens Professional software to enhance image clarity and resolution. The images presented are representative of the findings from five separate samples ($n = 5$). Scale bars shown in the images represent 10 μm, 20 μm or 50 μm. Super-resolution images (2D techniques) confirmed the co-localization of ferrylHb and CD163 receptor. Representative image, colocalization rate is the average value ± SD ($n = 4$).

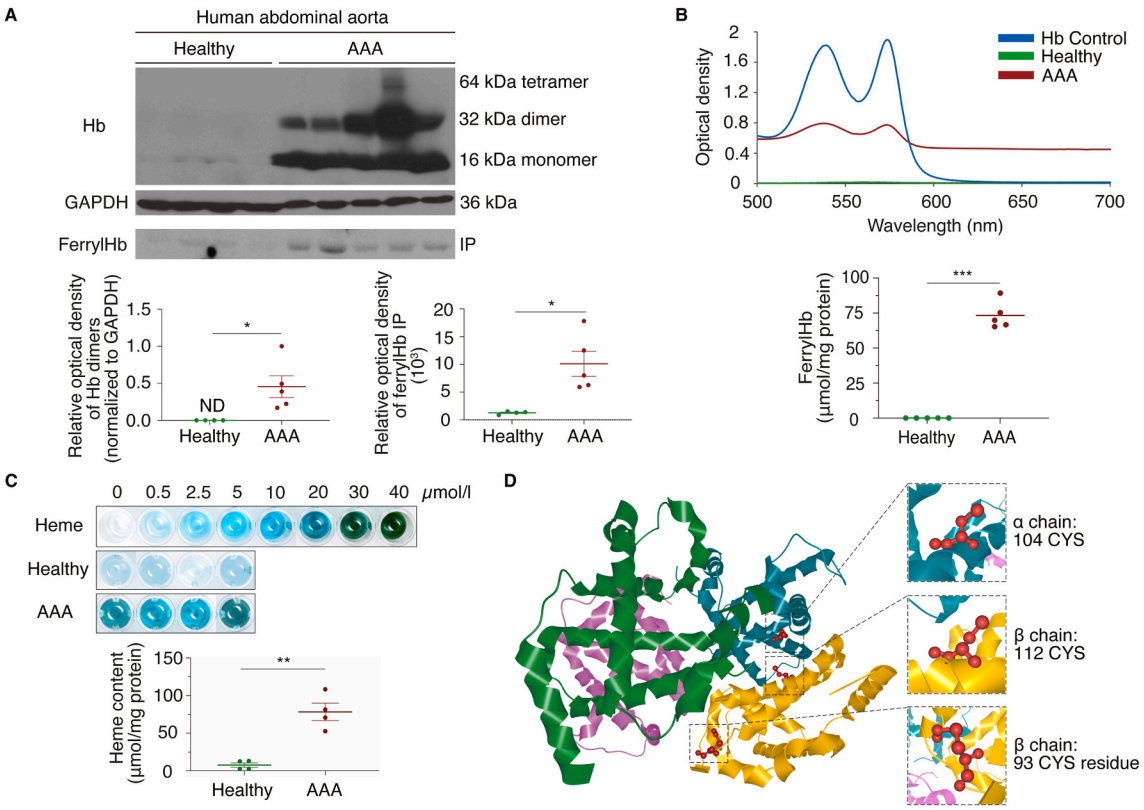

Fig. 2. Oxidative modification of hemoglobin and heme release in human abdominal aortic aneurysm tissues.
(**A**) The representative Western blot and immunoprecipitation (IP) analysis were performed to compare the levels of Hb dimers (upper panel) and ferrylHb (lower panel) between healthy aorta tissues ($n = 4$) and AAA tissues ($n = 5$). To detect Hb in healthy aorta and AAA tissues Western blot analysis was performed employing anti-human Hb antibody. The protein levels of Hb dimers were normalized to GAPDH. For IP of ferrylHb the pulldown was carried out using anti-human ferrylHb antibody then the same antibody was utilized for detection. Quantitative results for each protein group are presented, with data shown as the mean ± SEM for each group ($n = 4$ or 5 per group). $^{*}P < 0.05$ using unpaired *t*-test. (**B**) Spectral analysis of aortic tissue from healthy ($n = 5$), AAA ($n = 5$), and Hb control are shown. FerrylHb concentration was calculated. The results are shown as the mean values ± SEM of the experiments. $^{***}P < 0.001$ (unpaired *t*-test). (**C**) Total heme concentrations (μmol/mg protein) of human healthy ($n = 4$) and AAA ($n = 4$) abdominal aorta tissue lysates were determined spectrophotometrically and calculated according to the heme standard curve. $^{**}P < 0.01$ using unpaired *t*-test. (**D**) Trypsin-digested samples from human aortic aneurysm tissues ($n = 5$) were used for LC-MS/MS analysis to investigate the oxidation of cysteine (CYS) residues in Hb chains. The image illustrates the specific sites of CYS oxidation within the Hb α and β chains
α chain104 CYS, LLSHCLLVTLAAHLPAEFTPAVHASLDKFLASVSTVLTSK
β chain112 CYS, LLGNVLVCVLAHHFGK
β chain93 CYS residue, GTFATLSELHCDKLHVDPENFR
Human Hb was visualized with CAVER Analyst 2.0 software using RCSB PDB entry 1BUW. The mass spectrometry results are presented in Proteomics Data 1.

compared to those on STD (Fig. 3B and Supplemental Fig. 2B). Blood pressure levels did not differ between the two AngII-treated groups (Supplemental Fig. 3A). Control groups (STD and HFD without AngII) did not develop aneurysms. Based on previously established criteria [44], aneurysms were classified into four stages: I) normal aorta; II) aortic aneurysm without hemorrhage; III) aortic aneurysm with hemorrhage; and IV) ruptured aorta (Supplemental Fig. 3B). Notably, the incidence of hemorrhage ($n = 17/19$) and rupture ($n = 8/19$) was higher in AngII-treated mice on HFD compared to those on STD ($n = 9/19$ and $n = 4/19$, respectively) (Supplemental Fig. 3C and D).

Due to the fact that ferrylHb was found to accumulate in human hemorrhaged AAA, we tested whether AngII-induced AAA tissue specimens shared the same characteristics of Hb oxidation. Spectral analysis of Hb derived from hemorrhaged AAA samples showed peaks at 533 and 571 nm, indicating the presence of Hb. Oxidative states of Hb were quantified, showing that metHb and ferrylHb were more prevalent in hemorrhaged AAAs compared to ferroHb, particularly in HFD-fed mice (Fig. 3C). Additionally, Western blot analysis further supported the oxidation of Hb to the ferryl state, as evidenced by the formation of Hb dimers and the covalent crosslinking of globin chains in ApoE$^{-/-}$ mice treated with AngII on an HFD (Fig. 3D).

To further explore the oxidative alteration of the globin chain we determined oxidation hotspots of Hb in hemorrhaged mouse aneurysm tissue. Comparing to human aneurysms, where βCys93, βCys112, and αCys104 were identified to be critical for free radical-induced oxidation, we detected oxidation specifically at βCys93 (Fig. 3E and Proteomics Data 2).

As in human AAAs, the accumulation of oxidized Hb was accompanied by elevated heme levels in AAA tissue samples of HFD-fed mice treated with AngII (Fig. 3F).

Importantly, when ferrylHb and heme contents of the artery walls from human samples and from animal experimental groups are combined and evaluated by correlation analyses, a strong relationship can be observed between the ferrylHb concentrations and the free heme levels especially at extremely high values of ferrylHb in cases of hemorrhaged abdominal aneurisms ($R = 0.717$, $P = 0.030$) (Fig. 3G).

3.5. *Hemoglobin is taken up by neutrophils and macrophages in hemorrhaged abdominal aortic aneurysms in mice*

In cases of human AAA, neutrophils and macrophages internalize ferrylHb (Fig. 1). To determine whether a similar phenomenon occurs in

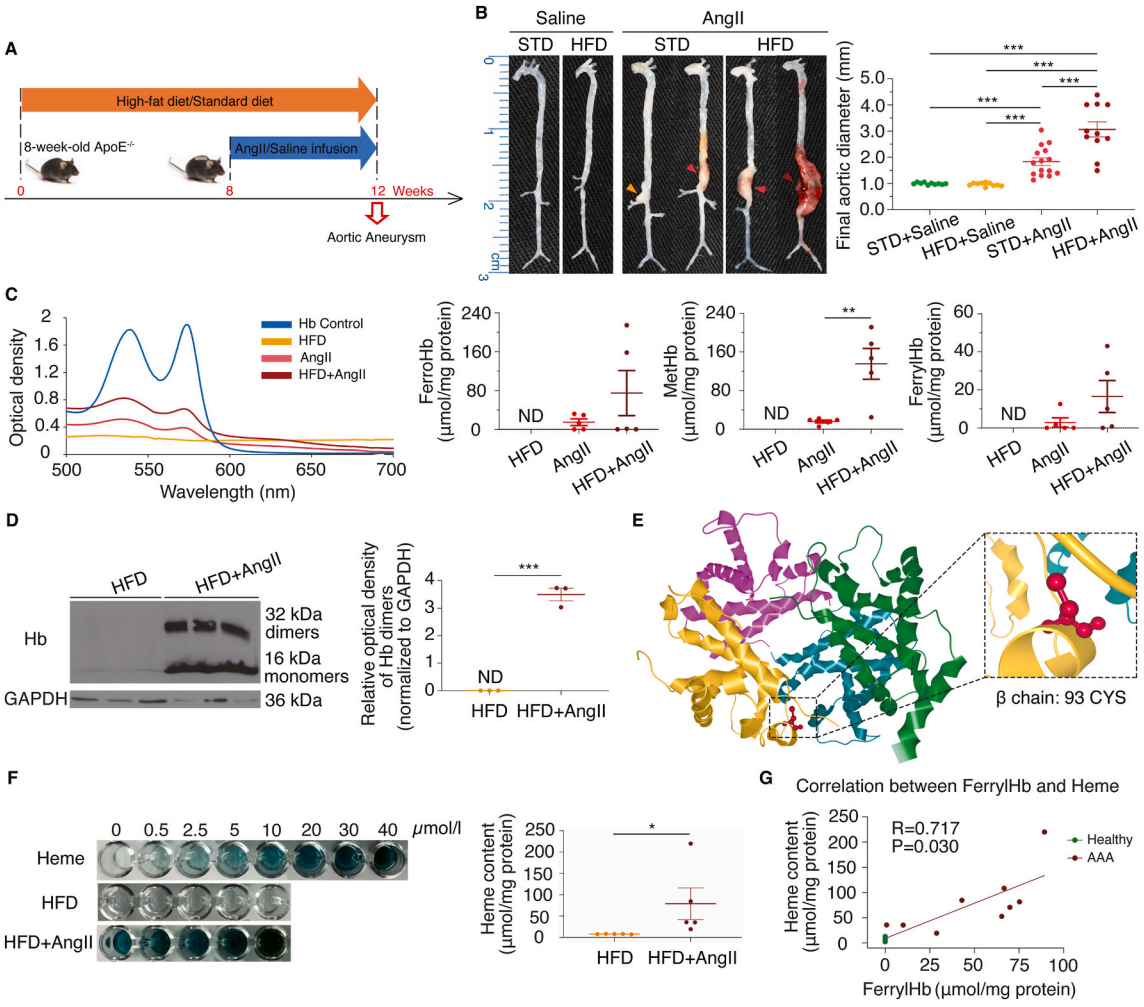

Fig. 3. Ferryl hemoglobin is present in abdominal aneurysms of mice on a high-fat diet treated with angiotensin II.
(**A**) Experimental Schema: 8-week-old ApoE$^{-/-}$ male mice were maintained on a high-fat diet (HFD) or a standard diet (STD) for a total duration of 12 weeks. During the last 4 weeks of feeding, they were implanted with osmotic pumps containing angiotensin II (AngII) or saline. (**B**) Representative photographs of aortic tissues in four groups of mice who received treatment with saline, AngII, saline plus HFD, and AngII plus HFD, respectively. Yellow triangles indicate an aortic aneurysm without hemorrhage; light red triangles indicate an aortic aneurysm with hemorrhage; dark red triangles indicate a ruptured aorta. Maximal suprarenal abdominal aortic diameter (in mm) measured from the isolated aorta at day 28 post-infusion; ***$P < 0.001$ (unpaired *t*-test). (**C**) Spectral analysis of aortic tissue from the following groups: Hb control, HFD, AngII, and HFD + AngII (AAA) ($n = 5$). The concentrations and ratios of ferroHb, metHb, and ferrylHb were calculated. Results are presented as mean values ± SEM. Statistical significance is indicated as follows: **$P < 0.01$ (unpaired *t*-test). ND, not detectable. (**D**) Representative Western blot of the HFD and HFD + AngII tissues using anti-Hb antibody. The expression levels of Hb dimers were assessed. The protein levels were normalized to GAPDH. Quantitative results for each protein group are presented, with data shown as the mean ± SEM for each group ($n = 3$ per group); ***$P < 0.001$, unpaired *t*-test. (**E**) Oxidation hotspots in the globin chains were identified in mouse aortic aneurysm tissue. Trypsin-digested samples from HFD + AngII-treated mice (aneurysms with rupture) were analyzed using LC-MS/MS ($n = 4$/group). The image highlights the location of CYS oxidation within the Hb chains. Specifically, the β chain at residue 93 (CYS) within the sequence GTFASLSELHCDKLHVDPENFR. Visualization of mouse Hb was conducted using CAVER Analyst 2.0 software, with structural data obtained from RCSB PDB entry 3HRW. The mass spectrometry results are presented in Proteomics Data 2. (**F**) Heme levels of AAA in mice on HFD ($n = 5$) and HFD + AngII ($n = 5$) were measured and quantified by the fluorescence assay; *$P < 0.05$ using an unpaired *t*-test. (**G**) The correlation between ferrylHb and heme content of aortic wall from humans and mice was assessed using Pearson's correlation analysis. Correlation coefficient (R) and *P* values were calculated. A two-tailed $P < 0.05$ was considered statistically significant.

our mouse model of the hemorrhaged aneurysm, we performed IHC staining to assess Hb uptake by neutrophils and macrophages in mouse AAA samples. Saline-treated mice exhibited normal morphology, with intact elastin layers in the suprarenal aortas, as confirmed by histological analysis using H&E and EVG staining. In contrast, AngII infusion induced AAA formation and significant elastin degradation in the aortic walls (Fig. 4A and Supplemental Fig. 4). HFD feeding further exacerbated these effects, increasing both cell number and the severity grade of elastin degradation in AngII-treated mice compared to those on a STD.

Histological analysis revealed that in the area of the ruptured aortic wall extracellular accumulation of Hb occurred and that was taken up by neutrophils (highlighted inside the rectangle) (Fig. 4B). Similarly, macrophages (Fig. 4C) were also positive for Hb in the ruptured lesion. Extending the treatment duration to 15 weeks led to the appearance of NETs in advanced aortic aneurysm tissues as indicated by the arrow in EVG-stained sections (Fig. 4C). The filamentous structures composed of decondensed chromatin (DNA) and granular proteins such as MPO are demonstrated in Fig. 4D.

3.6. Uptake of ferryl hemoglobin occurs via CD163 by neutrophils

CD163 is a member of the scavenger receptor superfamily class B of the first subgroup [45]. This receptor binds Hb-haptoglobin complexes, facilitating their internalization and subsequent lysosomal degradation

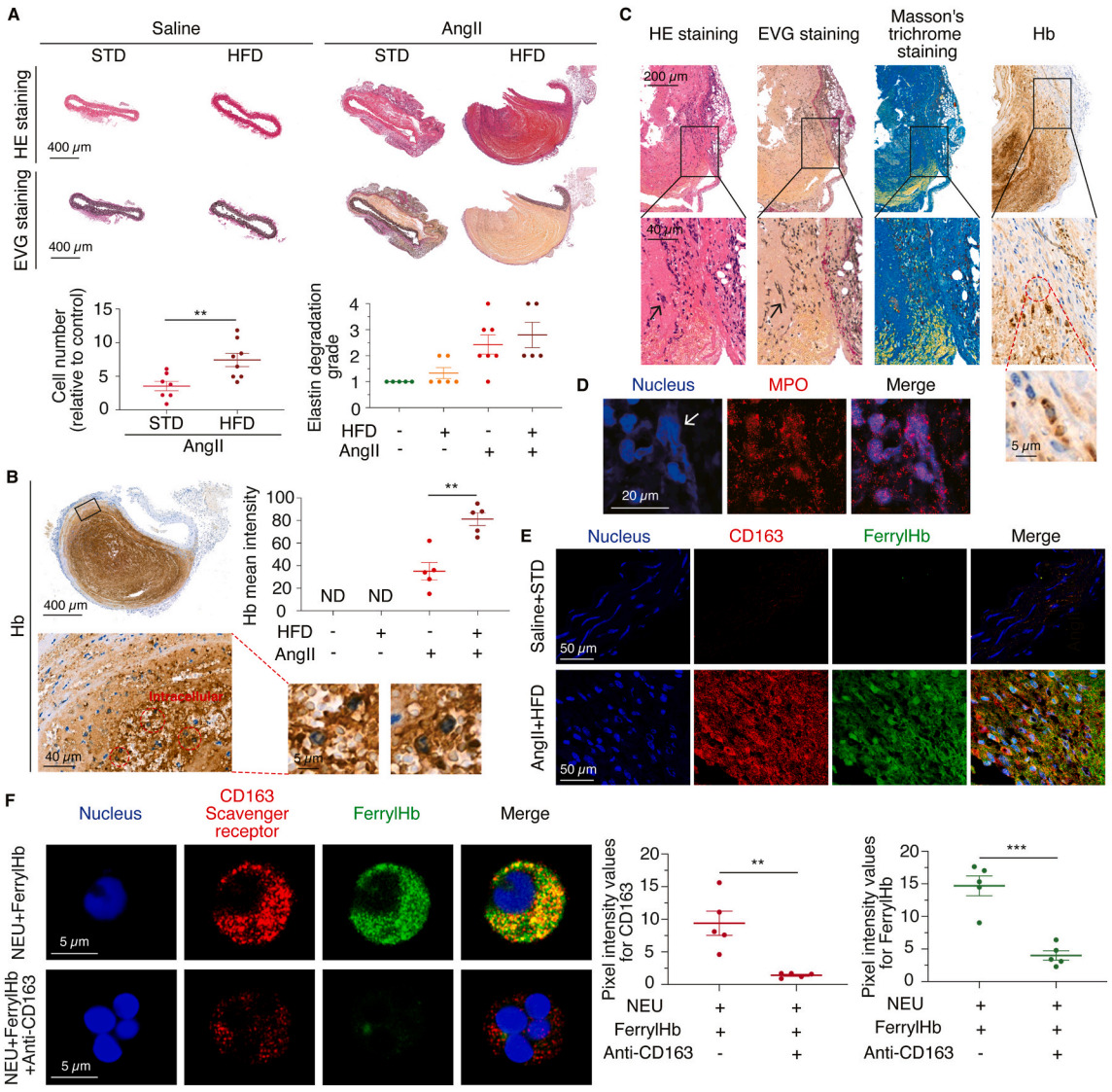

Fig. 4. Hemoglobin uptake by neutrophils and macrophages in hemorrhaged abdominal aortic aneurysms in mice.
(**A**) Mice were infused with AngII for 4 weeks and abdominal aortas were harvested for histological analysis. H&E and Verhoeff's elastin staining (EVG) of mouse AAA sections are shown. Cell number expressed as relative to the control ($n = 7$–8), $^{**}P < 0.01$ (unpaired *t*-test). Quantitative analysis of elastin degradation grade ($n = 5$–7). (**B**) Hb IHC staining of mouse AAA sections. Red dashed circles indicate intracellular Hb. High-magnification insets on the right highlight neutrophils exhibiting multilobed nuclei with intracellular cytoplasmic Hb staining. Quantitative analysis of Hb staining of tissue sections was performed using ImageJ software ($n = 5$). $^{**}P < 0.01$ (unpaired *t*-test). ND, not detectable. (**C**) H&E, EVG, Masson's trichrome, and Hb staining in advanced aortic aneurysm tissues. Red dashed circles inset on the right highlight intracellular Hb staining and round large single nucleus characteristics of macrophages. Lower panels provide higher magnification images with the arrow indicating neutrophil extracellular traps (NETs). (**D**) Mouse AAA (AngII + HFD) sections were stained with Hoechst 33,258 to visualize DNA (blue) and anti-MPO antibody conjugated with Alexa Fluor 647 to detect MPO (red). Images were captured using a Leica TCS SP8 gated STED-CW nanoscopic system and subsequently deconvolved with Huygens Professional software to enhance image clarity and resolution. Scale bars shown in the images represent 20 μm. The arrow indicates NETs. (**E**) FerrylHb and CD163-positive cells were detected by immunofluorescence staining in AAA (HFD + AngII) and in healthy aortas (STD + Saline) of mice. (**F**) Human neutrophils (NEUs) were isolated from the blood of healthy donors and subsequently treated with ferrylHb with or without anti-CD163 pretreatment for 16 h. The cells were then stained with Hoechst 33,258 for DNA (blue), an anti-ferrylHb antibody with Alexa Fluor 488 secondary antibody for ferrylHb (green), and CD163 antibody for the scavenger receptor (red). Images were acquired using a Leica TCS SP8 gated STED-CW nanoscopy and deconvolved using Huygens Professional software. Scale bars represent 5 μm. Pixel intensity for red color and green color were quantified using ImageJ software ($n = 5$). $^{**}P < 0.01$, $^{***}P < 0.001$ (unpaired *t*-test).

during hemolysis [46,47]. Importantly, it mediates non-inflammatory clearance of free, non oxidized Hb, thereby protecting tissues from oxidative stress.

We previously demonstrated that uptake of ferrylHb by macrophages occurs via CD163 even in the absence of haptoglobin [22]. As shown in Fig. 4E, a significant colocalization of CD163 and ferrylHb within neutrophils and macrophages was found in AngII- and HFD-induced AAA tissues. In contrast, such expression or colocalization was not detected in the aortas of healthy mice (Saline + STD).

To further test whether CD163 similarly mediates ferrylHb internalization in neutrophils, we conducted stimulated emission depletion microscopy (STED) nanoscopy (Fig. 4F). This analysis revealed significant co-localization of CD163 with ferrylHb in neutrophils. Further, pretreatment of cells with a CD163-blocking antibody resulted in a robust reduction of ferrylHb internalization, indicating that CD163 is critical for ferrylHb uptake in neutrophils. These findings strongly suggest that CD163 expressed in neutrophils mediates the uptake and clearance of ferrylHb.

3.7. Transcriptomic profile of human hemorrhaged abdominal aortic aneurysms is associated with inflammation and neutrophil activation

To further investigate the molecular mechanisms underlying AAA, we performed bulk RNA-seq analysis on aneurysmal and healthy aortic tissues to identify differentially expressed genes (DEGs) and associated pathways. Principal component analysis (PCA) revealed distinct transcriptomic profiles between AAA and healthy aortas, with biological replicates clustering closely together, explaining 55.45 % of the variation along PC1 (Fig. 5A).

In total, we identified 4327 DEGs, with 2473 genes significantly upregulated, and 1854 genes downregulated in AAA compared to healthy tissues (Fig. 5B; FDR<0.05, |log2FC|>1). The upregulated genes are largely associated with neutrophil activation, inflammation, calcification, apoptosis and iron metabolism. Gene Ontology (GO) enrichment analysis highlighted significant associations with biological processes such as "Neutrophil Chemotaxis", "Neutrophil Migration", and "Neutrophil Aggregation" (Fig. 5C). A more detailed assessment of neutrophil-related genes showed the upregulation of S100A8, ADAM8, DOCK8, and SELL, among others (Fig. 5D).

In addition to neutrophil activation pathways, several inflammatory genes, including IL1B, and IL6, were notably affected raising the potential of macrophage involvement. Calcification, apoptosis, and iron metabolism-related genes, including HBB, HMOX1, and LTF, were also significantly dysregulated in AAA samples compared to controls. These findings underscore the involvement of ferrylHb and neutrophil-mediated inflammation in the pathogenesis of AAA.

3.8. Ferryl hemoglobin induces transcriptomic changes in human macrophages that overlap with those observed in abdominal aortic aneurysms

To investigate the molecular impact of ferrylHb on macrophages in more detail and its potential involvement in AAA pathophysiology, we analyzed DEGs from human AAA biopsies and ferrylHb-treated human macrophages (8-h incubation). Comparative analysis revealed a significant overlap, with 884 shared DEGs-685 upregulated and 199 downregulated-between the two datasets (Fig. 6A). This corresponds to 57.18 % of upregulated and 23.78 % of downregulated DEGs from the ferrylHb-treated monocytes, suggesting that ferrylHb may drive the key transcriptomic changes observed in AAA in macrophages.

Notably, overlapping DEGs included genes involved in oxidative stress (HMOX1, HBA1), pro-inflammatory mediators (IL6, CCL8, CCL9), and matrix remodeling enzymes (MMPs) (Fig. 6B). To visualize the

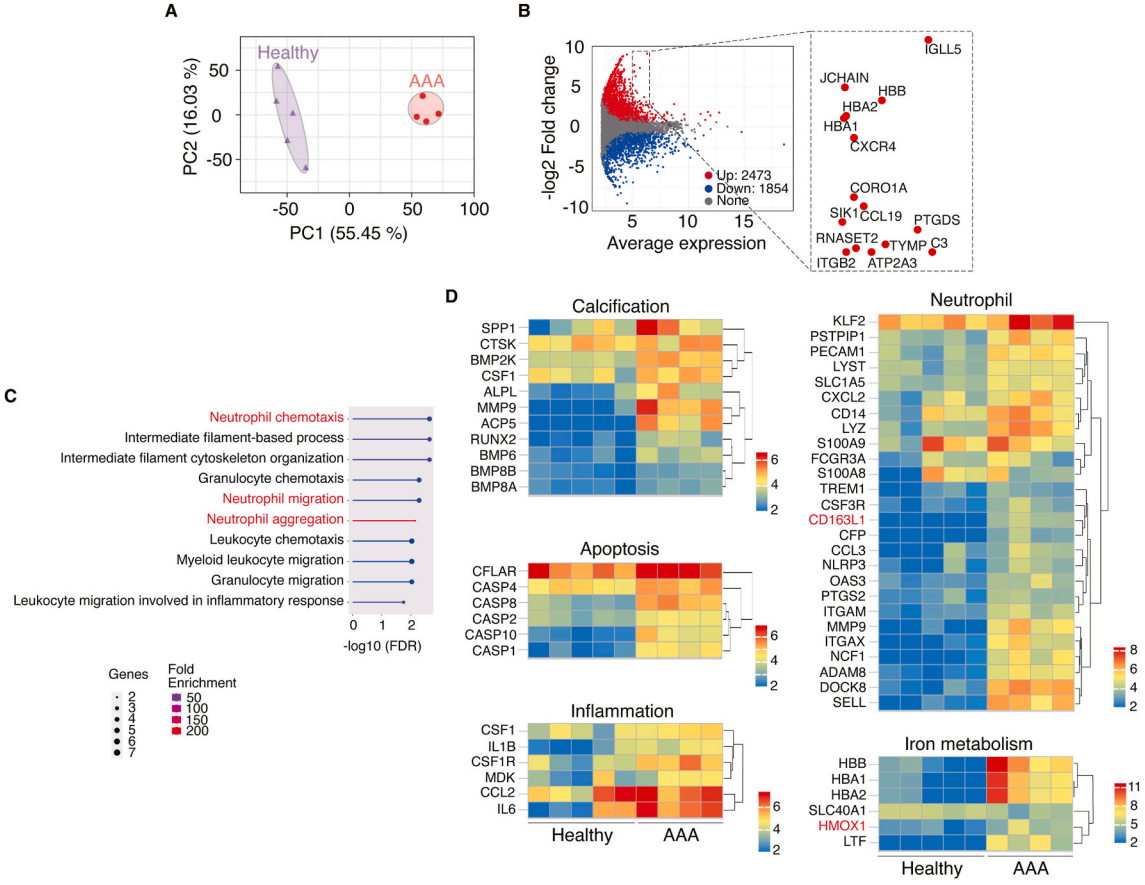

Fig. 5. Distinct transcriptomic profile between healthy aorta tissue and hemorrhaged abdominal aortic aneurysm in human.
(**A**) RNA-seq transcriptomic analysis was conducted on human aorta samples from healthy patients ($n = 5$, purple circle) and patients with AAA ($n = 4$, red circle). The principal component analysis (PCA) plot demonstrates the variance between these two groups. Unit variance scaling and singular value decomposition (SVD) with imputation were utilized to calculate the principal components. The X and Y axes represent principal component 1 (PC1) and principal component 2 (PC2), which account for 55.45 % and 16.03 % of the total variance, respectively. (**B**) The DEGs between healthy aorta and AAA are represented in a volcano plot. Red dots indicate upregulated genes, blue dots represent downregulated genes, and gray dots denote genes that are not differentially expressed. Inset highlights top upregulated DEGs. (**C**) The Gene Ontology (GO) enrichment analysis of DEGs focuses on the biological processes that are significantly affected. The overview displays the top 10 significantly enriched GO terms ranked by -log10 of the False Discovery Rate (FDR). These terms represent the biological processes that are most impacted by the DEGs in the context of healthy aorta versus AAA. A heatmap was generated to represent the expression levels of gene markers associated with specific pathways in healthy aorta and AAA samples. The heatmap is divided into three sections. (**D**) Targeted clustered analysis showing absolute expression patterns of genes associated with calcification, apoptosis, and inflammation, neutrophil, and iron metabolism from healthy and AAA groups.

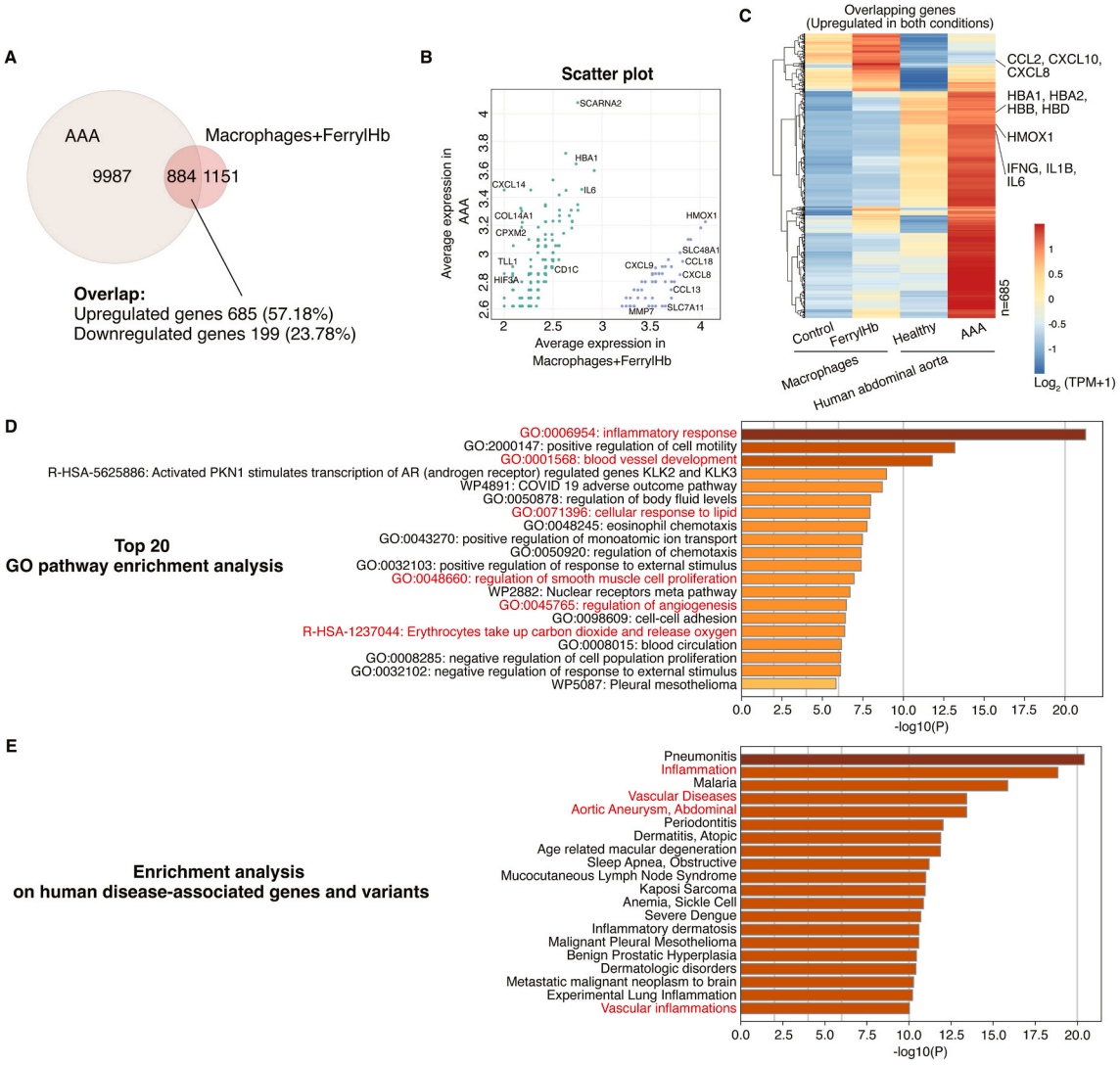

Fig. 6. Comparative analysis between human abdominal aortic aneurysms and human macrophages exposed to ferryl hemoglobin.
(**A**) Venn diagram of the DEGs identified from RNA-seq analysis of human AAA tissues vs healthy (yellow circle) and ferrylHb-treated macrophages (8h exposure) (red circle). The human macrophages used were derived from blood monocytes collected from healthy donors. (**B**) Scatter plot depicting the number of commonly regulated genes from each group comparison. The Y-axis shows the DEGs in the AAA versus healthy samples, and the X-axis shows the human macrophages treated with ferrylHb comparison. Data sets were filtered for logFC >2, and the top genes are labeled. (**C**) Clustered heatmap of upregulated genes (685 genes) belonging to the commonly regulated and overlapping gene set from the Venn diagram. The expression scale indicates $\log_2$ (TPM+1). (**D**) Top 20 GO pathway enrichment analysis on common overlapping DEGs in AAA when compared with healthy donors, and human macrophages treated with ferrylHb compared with control. All genes in the genome have been used as the enrichment background. Terms with a *P*-value <0.01, a minimum count of 3, and an enrichment factor >1.5 are collected and grouped into clusters based on their membership similarities. Kappa scores are used as the similarity metric when performing hierarchical clustering on the enriched terms, and sub-trees with a similarity of >0.3 are considered a cluster. The most statistically significant term within a cluster is chosen to represent the cluster. (**E**) Disease associations were assessed using human disease-associated genes and variants (DisGeNET). The figure displays the most significantly enriched disease terms, ranked by -$\log_{10}$(*P*-value), with terms grouped by semantic similarity. Only terms with adjusted *P*-value <0.05 were considered significant.

overlapping transcriptomic response, a heatmap was generated using the 685 consistent upregulated DEGs (Fig. 6C). Genes related to inflammatory signaling (IFNG, IL1B, IL6, CCL2, CXCL10, CXCL8) and iron metabolism (HMOX1, HBA1, HBA2, HBB, HBD) were highly upregulated in both datasets, further supporting the hypothesis that ferrylHb-mediated oxidative stress and immune activation are connected in AAA pathophysiology.

GO enrichment analysis further highlighted biological processes including inflammatory response, blood vessel development, and angiogenesis (Fig. 6D and Supplemental Table 1). Disease enrichment analysis using DisGeNET [48] via Metascape [49] identified significant associations with vascular and inflammatory diseases, including abdominal aortic aneurysm and vascular inflammation (Fig. 6E and Supplemental Table 2). To visualize relationships among enriched terms, a network plot was generated using Cytoscape 5. Nodes were colored by cluster ID (Supplemental Fig. 5A) and by statistical significance (Supplemental Fig. 5B).

3.9. Transcriptomic signatures of ruptured aneurysms in mice resemble those observed in human hemorrhagic aneurysms

To identify the genes and pathways that differ among the groups treated with HFD + AngII, STD + AngII, HFD + Saline, and STD + Saline (healthy aorta), we performed RNA-seq analysis. Despite the genetic variability commonly observed in human samples, the transcriptomic profiles of the HFD + AngII and STD + AngII groups were distinct, with biological replicates clustering together when compared to healthy tissue segments (Supplemental Fig. 6A).

In the comparison of HFD + Saline and HFD + AngII mice, 3056 DEGs were identified, including 1945 upregulated and 1111 downregulated genes (Supplemental Fig. 6B). Similarly, a comparison between STD + AngII and HFD + AngII samples revealed 2924 DEGs with 1569 genes upregulated and 1355 genes downregulated. Several of the top DEGs related to neutrophil function, such as S100A8 and S100A9, and inflammatory response cytokines like IL6, CCL7, IL1R2, and IL1B. Genes encoding various members of the hemoglobin family, including HBA-A1, HBA-A2, HBB-BT, and HBB-BS, were also differentially expressed.

An unbiased investigation using the GO database highlighted several affected pathways related to NET formation and inflammation, consistent with our findings in human aneurysm samples (Supplemental Fig. 6C). Further deconvolution of bulk RNA-seq data using Granulator, a cell composition matrix revealed that neutrophils represented the most abundant cell type (Supplemental Fig. 7). Targeted analysis of gene expression associated with neutrophils, inflammation, iron metabolism, calcification, and apoptosis indicated a greater severity of the aneurysms

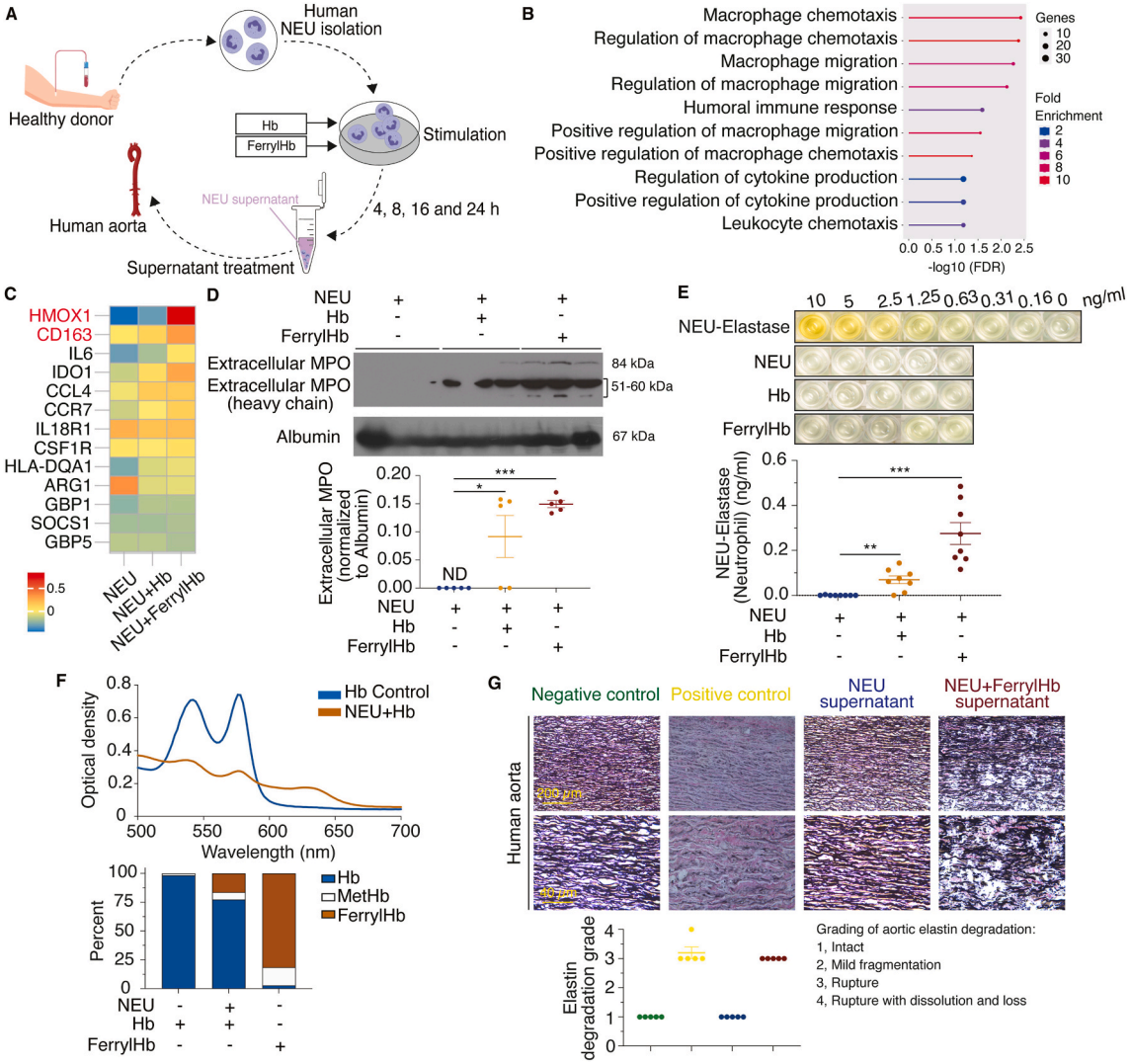

Fig. 7. Neutrophils activated by ferryl hemoglobin exhibit upregulation of genes associated with the recruitment of macrophages, liberation of elastase and myeloperoxidase, and aggravation of aortic elastin degradation.

(**A**) The experimental procedure is illustrated. Human neutrophils (NEU) were isolated from the blood of healthy donors and subsequently treated with 10 μmol/l Hb or 10 μmol/l ferrylHb. The cells were incubated for 4, 8, 16, or 24 h. RNA-seq transcriptomic analysis was performed on human neutrophils treated with Hb or ferrylHb for 4 h. To assess the effect of NEU-elastase on vascular extracellular matrix integrity, media (supernatants) from neutrophils were collected and incubated with human aortic tissue sections at room temperature overnight. Elastin degradation was subsequently evaluated. (**B**) Gene set enrichment of differentially expressed genes enriched in neutrophils treated by Hb or ferrylHb ($n = 5$). (**C**) Heatmap of differentially expressed genes associated with macrophages. Hierarchical clustering is also visualized ($n = 4$). (**D**) Expression levels of extracellular MPO were assessed. 20 μl of supernatant samples were analyzed for extracellular MPO and MPO heavy chain by Western blotting. For control, albumin (20 μl/lane) was used. Quantification of MPO is presented, with results shown as mean values ± SEM. Statistical significance was determined using an unpaired *t*-test: $^{*}P < 0.05$; $^{***}P < 0.001$ ($n = 5$/group). ND, not detected. (**E**) NEU-elastase release was quantified using an ELISA. 10 μl of each sample were added to a microwell plate and incubated. The absorbance was measured at 450 nm using a microplate reader. The concentrations of NEU-elastase were expressed as ng/ml. Statistical significance was determined using an unpaired *t*-test: $^{**}P < 0.01$, $^{***}P < 0.001$ ($n = 8$/group). (**F**) The concentrations of various redox states of Hb were determined by analyzing the visible spectra of the samples. The presence of different Hb redox states was calculated as a percentage of the total heme content. (**G**) Human aortic tissue sections were incubated overnight at room temperature with conditioned media from four groups: Negative control, DMEM culture medium only; Positive control, DMEM containing the 2 units/ml elastase; NEU supernatant, supernatant from untreated human NEU; NEU + ferrylHb supernatant, supernatant from neutrophils treated with ferrylHb ($n = 5$/group). Elastin integrity was assessed by EVG staining, and elastin degradation was scored using the following grading system: 1, Intact elastin; 2, Mild fragmentation; 3, Rupture; 4, Rupture with dissolution and loss of elastin fibers.

in the HFD + AngII group compared to the other experimental groups (Supplemental Fig. 6D).

3.10. Neutrophils are transcriptionally active under the stimulus of ferryl hemoglobin - upregulation of genes involved in the recruitment of macrophages

To investigate the potential relationship between Hb uptake by neutrophils in human and mouse aneurysms and the transcriptional changes observed at the tissue level, we performed RNA-Seq analysis on human neutrophils exposed to ferrylHb and ferroHb for 4 h (Fig. 7A). Gene set and GO network enrichment analysis (Fig. 7B and C) revealed differentially expressed pathways in neutrophils treated with ferrylHb or ferroHb. GO analysis identified several of these pathways as being associated with macrophage chemotaxis or migration. Additionally, GO analysis indicated that many of these DEGs are associated with processes involved in cell uptake and secretion, such as macrophage phagocytosis and endocytosis, which were among the top GO terms. Numerous DEGs identified between the control and treated groups were inflammatory genes, including several chemokine and cytokine genes previously found to be elevated in aneurysms (Supplemental Fig. 8).

3.11. Activation of neutrophils occurs in response to ferryl hemoglobin

To confirm the activation of neutrophils by ferrylHb, we measured the release of MPO (Fig. 7D) and neutrophil elastase (Fig. 7E) at 24 h. A

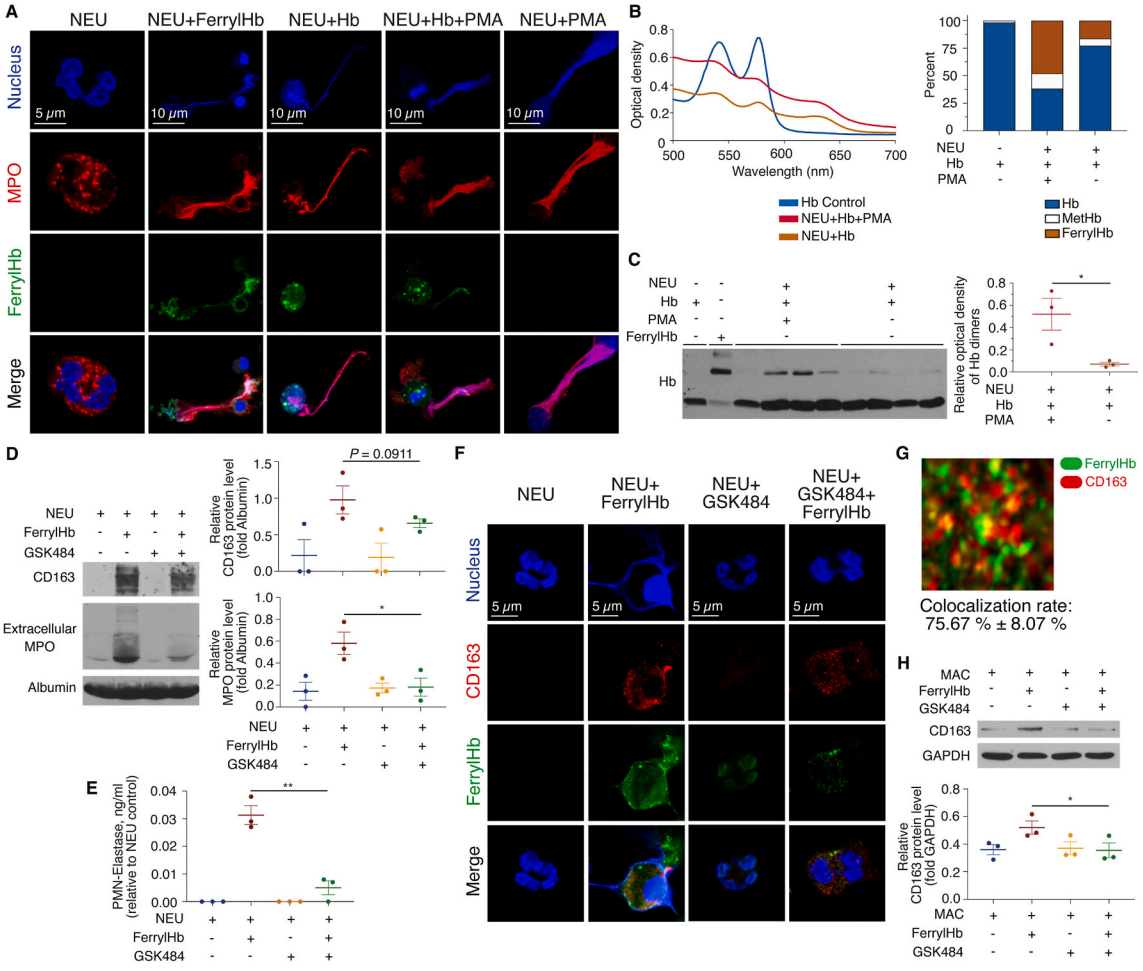

Fig. 8. Ferryl hemoglobin - induced NETosis occur via PAD4.
(**A**) Human neutrophils (NEUs) collected from healthy donors were stimulated under the following conditions: 10 μg/ml 12-myristate 13-acetate (PMA), 10 μg/ml PMA combined with 10 μmol/l Hb, 10 μmol/l Hb alone, or 10 μmol/l ferrylHb alone. NEUs were cultured on coverslips. Cells were stained with Hoechst 33,258 to visualize DNA (blue), an anti-MPO antibody conjugated with Alexa Fluor 647 to detect MPO (red), and an anti-ferrylHb antibody conjugated with Alexa Fluor 488 to identify ferrylHb (green). Imaging was performed using Leica TCS SP8 gated STED-CW nanoscopy, and images were subsequently deconvolved using Huygens Professional software. (**B**) The concentrations of various redox states of Hb were determined by analyzing the visible spectra of the samples. The presence of different Hb redox states was calculated as a percentage. (**C**) Hb was analyzed using an anti-Hb antibody. The Western blots show the presence of Hb and ferrylHb in NEUs. A quantitative analysis of Western blots was performed ($n = 3$); $^{*}P < 0.05$ (unpaired t-test). (**D**) Western blot analysis was performed to assess CD163 and extracellular MPO levels in supernatants. NEUs treated with peptidylarginine deiminase 4 (PAD4) inhibitor GSK484. For each lane, 37.5 μl of supernatant was loaded. Quantification of CD163 and MPO expression is presented as mean ± SEM ($n = 3$ per group). Statistical significance was determined by paired t-test, with $^{*}P < 0.05$ indicating significance. (**E**) NEU-elastase release was quantified using an ELISA. The absorbance was measured at 450 nm using a microplate reader. The concentrations of NEU-elastase were expressed as ng/ml. Statistical significance was determined using an unpaired t-test: $^{**}P < 0.01$ ($n = 3$/group). (**F**) Cells were stained with Hoechst 33,258 to visualize DNA (blue), an anti-CD163 antibody conjugated with Alexa Fluor 647 to detect CD163 (red), and an anti-ferrylHb antibody conjugated with Alexa Fluor 488 to identify ferrylHb (green). Imaging was performed using Leica TCS SP8 gated STED-CW nanoscopy, and images were subsequently deconvolved using Huygens Professional software. Scale bars shown in the images represent 5 μm. (**G**) Super-resolution images (2D techniques) confirmed the co-localization of ferrylHb and CD163 receptor. Representative image, colocalization rate is the average value ± SD, $n = 3$. (**H**) Western blot analysis was performed to assess CD163 expression in macrophages (MAC). MAC were treated with GSK484; for each lane, 20 μg of proteins were loaded. CD163 expression is presented as mean ± SEM ($n = 3$ per group). Statistical significance was evaluated using a paired t-test, with $^{*}P < 0.05$ considered significant.

robust release of MPO and elastase was observed in response to ferrylHb exposure. Importantly, exposing neutrophils to ferroHb for 24 h also elevated extracellular MPO levels and elastase, although to a lesser extent than ferrylHb. No extracellular MPO was detected in the control group.

Given previous reports indicating neutrophils can oxidize Hb [50,51], we tested whether this oxidation occurred during the 24-h exposure. As shown in Fig. 7F, ferrylHb constituted 16.26 % of total Hb at 24 h in the presence of neutrophils.

3.12. Ferryl hemoglobin induced elastase release from neutrophils degrades elastin in human aortic tissue

After ferrylHb exposure, the neutrophil supernatant was applied to human aortic tissue and incubated overnight at room temperature. As demonstrated in Fig. 7G, elastin fibers were fragmented in the human abdominal aorta as a result of treatment with the supernatant of ferrylHb stimulated neutrophils. In contrast, in the unstimulated neutrophil group, the elastic fibers were well organized throughout the wall.

3.13. Hemoglobin induces NETosis

Exposure of neutrophils to ferrylHb for 4 h induces a transcriptional response, and a subset of neutrophils exposed to both ferrylHb and ferroHb for prolonged periods (16–24 h) undergo cell death, as demonstrated in Supplemental Fig. 9. Since NETosis was observed in AAA in humans [16,19] and the formation of NETs was detected in our animal model of hemorrhaged AAA, we sought to determine whether Hb acts as a trigger for NETosis. As shown in Fig. 8A, both ferrylHb and ferroHb exposure resulted in the expulsion of NETs into the extracellular space, similar to the effect induced by phorbol 12-myristate 13-acetate (PMA), a known neutrophil activator [52–54]. Extracellular DNA, MPO, and ferrylHb were co-localized in NETs as visualized using STED nanoscopy. It's important to note ferrylHb was detected in neutrophils and trapped in NETs not only in experiments where ferrylHb was the inducer but also after exposure to Hb alone or in combination with PMA, indicating that Hb undergoes oxidation to ferrylHb. Furthermore, spectrophotometric analysis and Western blot analysis (Fig. 8B and C) confirmed the oxidation of Hb to ferrylHb by neutrophils, even in the absence of PMA, following 24 h of exposure.

3.14. Ferryl hemoglobin induced NETosis occur via PAD4

To further elucidate the regulatory mechanisms underlying ferrylHb-induced NETosis, we assessed the role of peptidylarginine deiminase 4 (PAD4), a key enzyme involved in chromatin decondensation during NET formation [55–57]. Immunofluorescence analysis demonstrated that treatment with GSK484, a selective PAD4 inhibitor, markedly suppressed the extracellular release of NETs following ferrylHb stimulation (Fig. 8F), indicating that PAD4 activity is essential for ferrylHb-induced NETosis.

In addition to its role in NET formation, PAD4 also regulates the release of extracellular MPO and elastase in response to ferrylHb (Fig. 8D and E). Western blot analysis showed a substantial increase in extracellular MPO levels upon ferrylHb treatment, which was significantly attenuated by GSK484-mediated PAD4 inhibition.

Moreover, ferrylHb stimulation led to an upregulation of CD163 expression in neutrophils (Fig. 8D). Importantly, PAD4 inhibition significantly reduced ferrylHb-induced CD163 expression. Immunofluorescence co-localization analysis further revealed a high degree of spatial overlap between ferrylHb and CD163 in neutrophils (75.67 % ± 8.07 %) (Fig. 8G), suggesting a potential interaction between ferrylHb signaling and CD163-mediated pathways. In line with the findings in neutrophils, ferrylHb-treated macrophages exhibited PAD4-dependent CD163 upregulation that was attenuated by GSK484, highlighting the importance of PAD4 in mediating ferrylHb-induced macrophage responses (Fig. 8H).

4. Discussion

Auto-oxidation of Hb is a continuous reaction that leads to metHb generation and concomitant formation of superoxide anions. Neutrophil and macrophage-derived reactive oxygen greatly amplifies Hb oxidation [21,22,25,26,37]. Both leukocytes are critically involved in the pathogenesis of AAA [5–8]. Since hemorrhage is documented in the pathology of several diseases, the question arises whether the interstitial bleeding and Hb oxidation represent only innocent bystander phenomenon or they contribute to the pathophysiology.

This study is the first that reveal the presence of oxidized Hb, ferrylHb, in the circulation in patients diagnosed with ruptured abdominal aneurysms who underwent open vascular surgery. The aim of our study was to identify the source of oxidation of Hb in the human hemorrhaged AAA leading to the generation of ferrylHb and describe its fate and pathophysiology. Significant generation of ferrylHb occurs within ruptured AAA in humans. Hb dimers, and tetramers were identified in the lesions in accordance with the formation of the ferryl state in the heme-iron moiety, accompanied by the formation of protein-based ferryl radicals. AngII-induced AAAs in ApoE$^{-/-}$ mice mimic human pathophysiology. We observed oxidation of the βCys93 residue of globin, and additionally, detected oxidation of βCys112 and αCys104 of Hb in human samples, confirming the presence of transient ferrylHb species as part of the AAA progression.

IHC analysis using anti-ferrylHb antibody revealed that ferrylHb is localized both extracellularly and also internalized by neutrophils and macrophages. FerrylHb-positive cells presented with morphological and immunophenotypic (MPO^{+}, NASD^{+}, CPM^{+}) features of neutrophils and macrophages in the hemorrhagic transformation lesions. Moreover, through unbiased genome-wide RNA-seq analysis in both human and murine models, we observed that hemorrhaged aneurysms are characterized by increased neutrophil and macrophage accumulation, conforming to previous observations [58–60].

Since ferrylHb accumulated extracellularly in the vessel wall of AAA is taken up by neutrophils in human and colocalized with CD163, we mimicked this in vivo finding by exposing human neutrophils to ferrylHb in cell culture. Immunofluorescent staining and two-dimensional images of Z-Stack-STED nanoscopy also presented a strong colocalization of ferrylHb and CD163 in neutrophils. Importantly, the CD163-blocking antibody led to a robust reduction of ferrylHb internalization. This study indicates that ferrylHb is taken up by neutrophils via CD163 receptor-mediated endocytosis independently of haptoglobin. This is in accordance with our previous findings exploring the CD163 receptor-mediated endocytosis of ferrylHb by macrophages independently from haptoglobin in atherosclerotic lesions [22].

CD163 was identified to act as a surface receptor and scavenges haptoglobin-Hb complexes via endocytosis by monocytes and macrophages providing the clearance of cell free Hb [47]. The plasma protein haptoglobin exhibiting strong Hb binding is essential for the clearance, and its depletion occurs during intravascular hemolysis [61]. The uptake of CD163-mediated haptoglobin-Hb complex was shown to determine protective and anti-inflammatory cellular responses in macrophages linked to heme oxygenase-1 (HO-1) [62] known to provide cytoprotective activities via mitigating apoptosis and inflammation, regulating vasomotor tone, and exerting antioxidant and immunomodulatory functions [21,63–65]. Therapeutic use of haptoglobin in disease states such as subarachnoid hemorrhage testifies its adaptive function in vascular biology [66]. Along this line of research Hb-haptoglobin complex was found to be a beneficial stimulus for macrophage differentiation as Hb or conditioned medium from adventitial human AAA promoted differentiation towards high CD163 expressing macrophages, with enhanced Hb uptake, increased anti-inflammatory cytokine secretion and decreased pro-inflammatory cytokine release [67]. Furthermore a high aneurysmal CD163 expression was connected to increase in

HO-1 level [68]. Hb was found to be also beneficial stimulus for macrophage differentiation in human atherosclerotic plaques to retard foam cell formation involving CD163 [69], restrain vascular calcification [70]. CD163 deficiency was shown to increase foam cell formation and plaque progression in atherosclerotic mice [71]. On the contrary, substantial evidence exist that support the pathophysiologic role of Hb-stimulated macrophages as promoter for the progression of atherosclerosis in ruptured atherosclerotic plaques [22,72]. The contradiction between the two described effects of Hb is presumably based on how the vessel wall microenvironment modifies the oxidative state of the free Hb in the extracellular space.

Here we observed that rapid formation of ferrylHb occurs as extracellular Hb exposed to leukocytes. The Hb composition related to its oxidative state within ruptured vascular lesions reshapes the polarization of macrophages and activation of neutrophils. We observed a significant oxidation of Hb both in human hemorrhagic aneurysms and in AngII provoked AAA in mice. The extent of oxidation of Hb in complicated atherosclerotic lesions was found to be even more pronounced [22] preventing the binding to haptoglobin and the subsequent CD163-dependent adaptive cellular responses. Instead, alarm signals and maladaptation occurs, such as inflammatory activation, NETosis and extracellular matrix degradation connected to exposure of neutrophils and macrophages to ferrylHb. Although, our data suggest that CD163 mediates ferrylHb-provoked processes, the causal role of CD163 remains incompletely established. Employing CD163-deficient mice in the AngII provoked AAA model, as our future plan, will provide direct mechanistic evidence whether CD163 is functionally required for ferrylHb-mediated AAA development.

It has been shown previously that PAD4 is essential for NET-mediated antibacterial function of neutrophils after stimulation with chemokines or incubation with bacteria [73]. Drawing in line, we also observed the involvement of PAD4 in extracellular release of NETs, MPO, and elastase in response to ferrylHb. To our surprise, the increased expression of CD163 by ferrylHb was found to be dependent on PAD4 as well both in neutrophils and macrophages. Further experiments are needed to explore the mechanism by which CD163 is connected to PAD4.

FerrylHb was previously demonstrated to target not only leukocytes but endothelium as well and subsequently trigger endothelial dysfunction and proinflammatory responses [39]. Rearrangement of the actin cytoskeleton, increased endothelial permeability and enhanced endothelial adhesion of monocytes were observed. Whether this interaction exists in AAA remained unestablished.

In the present study we demonstrate an interplay between neutrophils and macrophages with Hb in AAA leading to the accumulation of ferrylHb in intramural hemorrhages resulting in a subsequent cellular activations. FerrylHb polarized neutrophils exhibit increased transcriptional activity towards proinflammatory programming, degranulation, liberation of elastase and MPO, and NETosis, while macrophages polarized by ferrylHb drive inflammation, calcification, apoptosis, tissue remodeling, factors previously revealed to be involved in the development of AAA [11,74–76]. We conclude that oxidation of Hb to ferrylHb in hemorrhaged AAA provides a novel pathophysiological pathway related to red blood cell infiltration and Hb liberation, that contributes to the progression of AAA.

CRediT authorship contribution statement

Yuchao Ding: Conceptualization, Data curation, Formal analysis, Investigation, Methodology, Software, Validation, Visualization, Writing – original draft, Writing – review & editing. **László Potor:** Conceptualization, Data curation, Formal analysis, Methodology, Validation, Writing – original draft, Writing – review & editing. **Éva Katona:** Data curation, Formal analysis, Investigation, Methodology. **Péter Sótonyi:** Data curation, Formal analysis, Resources. **Ágnes Szappanos:** Data curation, Formal analysis, Methodology, Writing – review & editing. **Gergő Péter Gyurok:** Data curation, Formal analysis, Investigation. **Gábor Méhes:** Formal analysis, Project administration, Resources, Supervision. **Zoltán Hendrik:** Data curation, Formal analysis, Investigation, Methodology. **Attila Fintha:** Data curation, Formal analysis, Methodology. **Péter Attila Gergely:** Project administration, Resources, Validation. **Zoltán Benyó:** Data curation, Investigation. **Zsolt Combi:** Data curation, Formal analysis, Validation. **Katalin Éva Sikura:** Software, Validation, Visualization. **Lívia Beke:** Data curation, Investigation, Methodology. **Norbert Nemeth:** Resources, Supervision, Visualization. **Szabo Balazs:** Software, Validation, Visualization. **Ibolya Fürtös:** Investigation, Methodology, Software. **Gergő Kalló:** Investigation, Methodology. **Éva Csősz:** Conceptualization, Project administration, Resources, Software, Validation. **Szilárd Póliska:** Data curation, Formal analysis, Investigation. **Andreas Patsalos:** Data curation, Formal analysis, Methodology, Software, Visualization, Writing – review & editing. **E Sebastian Debus:** Conceptualization, Resources, Supervision, Validation, Writing – review & editing. **László Nagy:** Conceptualization, Funding acquisition, Project administration, Resources, Supervision, Validation, Writing – review & editing. **György Balla:** Conceptualization, Funding acquisition, Project administration, Supervision, Writing – review & editing. **József Balla:** Conceptualization, Funding acquisition, Investigation, Project administration, Resources, Supervision, Validation, Writing – original draft, Writing – review & editing.

Declaration of competing interest

All the authors declared no competing interests.

Acknowledgments

The research group is supported by HUN-REN-DE (11003) and NKFIH ADVANCED 149734 (J.B.). The project was co-financed by the European Union and the European Social Fund: EFOP-3.6.2-16-2017-00006 (LIVE LONGER). Project no. TKP2021-EGA-18 has been implemented with the support provided by the Ministry of Innovation and Technology of Hungary from the National Research, Development and Innovation Fund, financed under the TKP2021-EGA funding scheme. Y. D. was supported by the National Scholarship Program for international study of the China Scholarship Council, and the Tempus Public Foundation Stipendium Hungaricum Scholarship. L.P. was supported by the János Bolyai Research Scholarship of the Hungarian Academy of Sciences. The work was carried out at the University of Debrecen, Kálmán Laki Doctoral School of Biomedical and Clinical Sciences. Supported by the EKÖP-24-4 (Y.D. and L.P.) University Research Scholarship Program of the Ministry for Culture and Innovation from the source of the National Research, Development and Innovation Fund. L.N. was supported by R01AI185363 from the National Institutes of Health (NIH).

Appendix A. Supplementary data

Supplementary data to this article can be found online at https://doi.org/10.1016/j.redox.2025.103908.

Data availability

The RNA-seq data under this study are available in the NCBI BioProject database under accession number PRJNA1196652, PRJNA1196699, PRJNA594843, and PRJNA1196670. The proteomics data are available at the MassIVE database under accession number MSV000099477 and MSV000099478.

References

[1] R. Erbel, V. Aboyans, C. Boileau, E. Bossone, R.D. Bartolomeo, H. Eggebrecht, et al., 2014 ESC guidelines on the diagnosis and treatment of aortic diseases: document

covering acute and chronic aortic diseases of the thoracic and abdominal aorta of the adult. The task force for the diagnosis and treatment of aortic diseases of the european society of cardiology (ESC), Eur. Heart J. 35 (41) (2014) 2873–2926.
[2] P. Song, Y. He, D. Adeloye, Y. Zhu, X. Ye, Q. Yi, et al., The global and regional prevalence of abdominal aortic aneurysms: a systematic review and modeling analysis, Ann. Surg. 277 (6) (2023) 912–919.
[3] Z. Wang, Y. You, Z. Yin, Q. Bao, S. Lei, J. Yu, et al., Burden of Aortic Aneurysm and its attributable risk factors from 1990 to 2019: an Analysis of the Global burden of Disease Study 2019, Front. Cardiovasc. Med. 9 (2022) 901225.
[4] R.A. Quintana, W.R. Taylor, Cellular mechanisms of aortic aneurysm Formation, Circ. Res. 124 (4) (2019) 607–618.
[5] J.L. Eliason, K.K. Hannawa, G. Ailawadi, I. Sinha, J.W. Ford, M.P. Deogracias, et al., Neutrophil depletion inhibits experimental abdominal aortic aneurysm formation, Circulation 112 (2) (2005) 232–240.
[6] K.K. Hannawa, J.L. Eliason, D.T. Woodrum, C.G. Pearce, K.J. Roelofs, V. Grigoryants, et al., L-selectin-mediated neutrophil recruitment in experimental rodent aneurysm formation, Circulation 112 (2) (2005) 241–247.
[7] Z. Yuan, L. Shu, J. Fu, P. Yang, Y. Wang, J. Sun, et al., Single-Cell RNA sequencing deconstructs the distribution of immune cells within abdominal aortic aneurysms in mice, Arterioscler. Thromb. Vasc. Biol. 44 (9) (2024) 1986–2003.
[8] Y. Wang, Z. Liu, S. Song, J. Wang, C. Jin, L. Jia, et al., IRF5 governs macrophage adventitial infiltration to fuel abdominal aortic aneurysm formation, JCI Insight 9 (3) (2024).
[9] J.R. Stone, P. Bruneval, A. Angelini, G. Bartoloni, C. Basso, L. Batoroeva, et al., Consensus statement on surgical pathology of the aorta from the Society for Cardiovascular Pathology and the Association for European Cardiovascular Pathology: I. Inflammatory diseases, Cardiovasc. Pathol. 24 (5) (2015) 267–278.
[10] A. Chrysanthopoulou, E. Gkaliagkousi, A. Lazaridis, S. Arelaki, P. Pateinakis, M. Ntinopoulou, et al., Angiotensin II triggers release of neutrophil extracellular traps, linking thromboinflammation with essential hypertension, JCI Insight 6 (18) (2021).
[11] M.D. Tilson 3rd, The polymorphonuclear leukocyte and the abdominal aortic aneurysm: a neglected cell type and a neglected disease, Circulation 112 (2) (2005) 154–156.
[12] J. Klopf, C. Brostjan, C. Neumayer, W. Eilenberg, Neutrophils as regulators and biomarkers of cardiovascular inflammation in the context of abdominal aortic aneurysms, Biomedicines 9 (9) (2021).
[13] J. Huang, H. Liu, Z. Liu, Z. Wang, H. Xu, Z. Li, et al., Inhibition of aortic CX3CR1+ macrophages mitigates thoracic aortic aneurysm progression in Marfan syndrome in mice, J. Clin. Investig. 135 (2) (2025).
[14] V. Brinkmann, U. Reichard, C. Goosmann, B. Fauler, Y. Uhlemann, D.S. Weiss, et al., Neutrophil extracellular traps kill bacteria, Science 303 (5663) (2004) 1532–1535.
[15] H. Yan, H.F. Zhou, A. Akk, Y. Hu, L.E. Springer, T.L. Ennis, et al., Neutrophil proteases promote experimental abdominal aortic aneurysm via extracellular trap release and plasmacytoid dendritic cell activation, Arterioscler. Thromb. Vasc. Biol. 36 (8) (2016) 1660–1669.
[16] S. Yang, L. Chen, Z. Wang, J. Chen, Q. Ni, X. Guo, et al., Neutrophil extracellular traps induce abdominal aortic aneurysm formation by promoting the synthetic and proinflammatory smooth muscle cell phenotype via Hippo-YAP pathway, Transl. Res. 255 (2023) 85–96.
[17] C. Silvestre-Roig, Q. Braster, K. Wichapong, E.Y. Lee, J.M. Teulon, N. Berrebeh, et al., Externalized histone H4 orchestrates chronic inflammation by inducing lytic cell death, Nature 569 (7755) (2019) 236–240.
[18] J.S. Knight, W. Luo, A.A. O'Dell, S. Yalavarthi, W. Zhao, V. Subramanian, et al., Peptidylarginine deiminase inhibition reduces vascular damage and modulates innate immune responses in murine models of atherosclerosis, Circ. Res. 114 (6) (2014) 947–956.
[19] A.K. Meher, M. Spinosa, J.P. Davis, N. Pope, V.E. Laubach, G. Su, et al., Novel role of IL (Interleukin)-1 beta in neutrophil extracellular trap Formation and abdominal aortic aneurysms, Arterioscler. Thromb. Vasc. Biol. 38 (4) (2018) 843–853.
[20] M.P. Bonaca, P.T. O'Gara, Diagnosis and management of acute aortic syndromes: dissection, intramural hematoma, and penetrating aortic ulcer, Curr. Cardiol. Rep. 16 (10) (2014) 536.
[21] J. Balla, H.S. Jacob, G. Balla, K. Nath, J.W. Eaton, G.M. Vercellotti, Endothelial-cell heme uptake from heme proteins: induction of sensitization and desensitization to oxidant damage, Proc. Natl. Acad. Sci. U. S. A. 90 (20) (1993) 9285–9289.
[22] L. Potor, Z. Hendrik, A. Patsalos, E. Katona, G. Mehes, S. Poliska, et al., Oxidation of hemoglobin drives a proatherogenic polarization of macrophages in human atherosclerosis, Antioxidants Redox Signal. 35 (12) (2021) 917–950.
[23] J.F. Gibson, D.J.E. Ingram, Location of free electrons in porphin ring complexes, Nature 178 (4538) (1956) 871–872.
[24] S. Harel, J. Kanner, The generation of ferryl or hydroxyl radicals during interaction of haemproteins with hydrogen peroxide, Free Radic. Res. Commun. 5 (1) (1988) 21–33.
[25] F. Meng, A.I. Alayash, Determination of extinction coefficients of human hemoglobin in various redox states, Anal. Biochem. 521 (2017) 11–19.
[26] R.P. Patel, D.A. Svistunenko, V.M. Darley-Usmar, M.C. Symons, M.T. Wilson, Redox cycling of human methaemoglobin by H2O2 yields persistent ferryl iron and protein based radicals, Free Radic. Res. 25 (2) (1996) 117–123.
[27] P. Ren, M. Hughes, S. Krishnamoorthy, S. Zou, L. Zhang, D. Wu, et al., Critical role of ADAMTS-4 in the development of sporadic aortic aneurysm and dissection in mice, Sci. Rep. 7 (1) (2017) 12351.
[28] A. Daugherty, M.W. Manning, L.A. Cassis, Angiotensin II promotes atherosclerotic lesions and aneurysms in apolipoprotein E-deficient mice, J. Clin. Investig. 105 (11) (2000) 1605–1612.
[29] J.L. Tan, P.A. Davlouros, K.P. McCarthy, M.A. Gatzoulis, S.Y. Ho, Intrinsic histological abnormalities of aortic root and ascending aorta in tetralogy of Fallot: evidence of causative mechanism for aortic dilatation and aortopathy, Circulation 112 (7) (2005) 961–968.
[30] G. Silva, V. Jeney, A. Chora, R. Larsen, J. Balla, M.P. Soares, Oxidized hemoglobin is an endogenous proinflammatory agonist that targets vascular endothelial cells, J. Biol. Chem. 284 (43) (2009) 29582–29595.
[31] C.C. Winterbourn, Oxidative reactions of hemoglobin, Methods Enzymol. 186 (1990) 265–272.
[32] F.T. Meng, A.I. Alayash, Determination of extinction coefficients of human hemoglobin in various redox states, Anal. Biochem. 521 (2017) 11–19.
[33] N.T. Huy, D.T. Xuan Trang, D.T. Uyen, M. Sasai, S. Harada, K. Kamei, An improved colorimetric method for quantitation of heme using tetramethylbenzidine as substrate, Anal. Biochem. 344 (2) (2005) 289–291.
[34] T. Gall, D. Petho, A. Nagy, Z. Hendrik, G. Mehes, L. Potor, et al., Heme induces endoplasmic reticulum stress (HIER stress) in Human aortic smooth muscle cells, Front. Physiol. 9 (2018) 1595.
[35] J. Cox, M. Mann, MaxQuant enables high peptide identification rates, individualized p.p.b.-range mass accuracies and proteome-wide protein quantification, Nat. Biotechnol. 26 (12) (2008) 1367–1372.
[36] F.M. Cavaliere, A. Prezzo, C. Bilotta, M. Iacobini, I. Quinti, The lack of BTK does not impair monocytes and polymorphonuclear cells functions in X-linked agammaglobulinemia under treatment with intravenous immunoglobulin replacement, PLoS One 12 (4) (2017) e0175961.
[37] D. Lau, H. Mollnau, J.P. Eiserich, B.A. Freeman, A. Daiber, U.M. Gehling, et al., Myeloperoxidase mediates neutrophil activation by association with CD11b/CD18 integrins, Proc. Natl. Acad. Sci. U. S. A. 102 (2) (2005) 431–436.
[38] M. Korai, J. Purcell, Y. Kamio, K. Mitsui, H. Furukawa, K. Yokosuka, et al., Neutrophil extracellular traps promote the development of intracranial Aneurysm rupture, Hypertension 77 (6) (2021) 2084–2093.
[39] N. Posta, E. Csosz, M. Oros, D. Petho, L. Potor, G. Kallo, et al., Hemoglobin oxidation generates globin-derived peptides in atherosclerotic lesions and intraventricular hemorrhage of the brain, provoking endothelial dysfunction, Lab. Invest. 100 (7) (2020) 986–1002.
[40] A.I. Alayash, betaCysteine 93 in human hemoglobin: a gateway to oxidative stability in health and disease, Lab. Invest. 101 (1) (2021) 4–11.
[41] S. Jana, M.B. Strader, A.I. Alayash, The Providence mutation (betaK82D) in human hemoglobin substantially reduces betaCysteine 93 oxidation and oxidative stress in endothelial cells, Int. J. Mol. Sci. 21 (24) (2020).
[42] T. Pimenova, C.P. Pereira, P. Gehrig, P.W. Buehler, D.J. Schaer, R. Zenobi, Quantitative mass spectrometry defines an oxidative hotspot in hemoglobin that is specifically protected by haptoglobin, J. Proteome Res. 9 (8) (2010) 4061–4070.
[43] Y. Jia, P.W. Buehler, R.A. Boykins, R.M. Venable, A.I. Alayash, Structural basis of peroxide-mediated changes in human hemoglobin: a novel oxidative pathway, J. Biol. Chem. 282 (7) (2007) 4894–4907.
[44] V.S. Ramanath, J.K. Oh, T.M. Sundt 3rd, K.A. Eagle, Acute aortic syndromes and thoracic aortic aneurysm, Mayo Clin. Proc. 84 (5) (2009) 465–481.
[45] G. Onofre, M. Kolackova, K. Jankovicova, J. Krejsek, Scavenger receptor CD163 and its biological functions, Acta Med. 52 (2) (2009) 57–61.
[46] M.J. Nielsen, C.B. Andersen, S.K. Moestrup, CD163 binding to haptoglobin-hemoglobin complexes involves a dual-point electrostatic receptor-ligand pairing, J. Biol. Chem. 288 (26) (2013) 18834–18841.
[47] M. Kristiansen, J.H. Graversen, C. Jacobsen, O. Sonne, H.J. Hoffman, S.K. Law, et al., Identification of the haemoglobin scavenger receptor, Nature 409 (6817) (2001) 198–201.
[48] J. Pinero, A. Bravo, N. Queralt-Rosinach, A. Gutierrez-Sacristan, J. Deu-Pons, E. Centeno, et al., DisGeNET: a comprehensive platform integrating information on human disease-associated genes and variants, Nucleic Acids Res. 45 (D1) (2017) D833–D839.
[49] Y. Zhou, B. Zhou, L. Pache, M. Chang, A.H. Khodabakhshi, O. Tanaseichuk, et al., Metascape provides a biologist-oriented resource for the analysis of systems-level datasets, Nat. Commun. 10 (1) (2019) 1523.
[50] C.C. Winterbourn, A.J. Kettle, Redox reactions and microbial killing in the neutrophil phagosome, Antioxidants Redox Signal. 18 (6) (2013) 642–660.
[51] M. Minetti, C. Mallozzi, G. Scorza, M.D. Scott, F.A. Kuypers, B.H. Lubin, Role of oxygen and carbon radicals in hemoglobin oxidation, Arch. Biochem. Biophys. 302 (1) (1993) 233–244.
[52] H. Takei, A. Araki, H. Watanabe, A. Ichinose, F. Sendo, Rapid killing of human neutrophils by the potent activator phorbol 12-myristate 13-acetate (PMA) accompanied by changes different from typical apoptosis or necrosis, J. Leukoc. Biol. 59 (2) (1996) 229–240.
[53] O. Rodriguez-Espinosa, O. Rojas-Espinosa, M.M. Moreno-Altamirano, E.O. Lopez-Villegas, F.J. Sanchez-Garcia, Metabolic requirements for neutrophil extracellular traps formation, Immunology 145 (2) (2015) 213–224.
[54] D. Domer, T. Walther, S. Moller, M. Behnen, T. Laskay, Neutrophil extracellular traps activate proinflammatory functions of human neutrophils, Front. Immunol. 12 (2021) 636954.
[55] B. Wang, X. Su, B. Zhang, S. Pan, GSK484, an inhibitor of peptidyl arginine deiminase 4, increases the radiosensitivity of colorectal cancer and inhibits neutrophil extracellular traps, J. Gene Med. 25 (9) (2023) e3530.
[56] L. Wei, X. Wang, M. Luo, H. Wang, H. Chen, C. Huang, The PAD4 inhibitor GSK484 enhances the radiosensitivity of triple-negative breast cancer, Hum. Exp. Toxicol. 40 (7) (2021) 1074–1083.
[57] O.E. Sorensen, N. Borregaard, Neutrophil extracellular traps - the dark side of neutrophils, J. Clin. Investig. 126 (5) (2016) 1612–1620.

[58] N. Ibrahim, S. Bleichert, J. Klopf, G. Kurzreiter, H. Hayden, V. Knobl, et al., Reducing abdominal aortic aneurysm progression by blocking neutrophil extracellular traps depends on thrombus Formation, JACC Basic Transl Sci 9 (3) (2024) 342–360.
[59] J. Raffort, F. Lareyre, M. Clement, R. Hassen-Khodja, G. Chinetti, Z. Mallat, Monocytes and macrophages in abdominal aortic aneurysm, Nat. Rev. Cardiol. 14 (8) (2017) 457–471.
[60] T. Hadi, L. Boytard, M. Silvestro, D. Alebrahim, S. Jacob, J. Feinstein, et al., Macrophage-derived netrin-1 promotes abdominal aortic aneurysm formation by activating MMP3 in vascular smooth muscle cells, Nat. Commun. 9 (1) (2018) 5022.
[61] T. Wada, H. Oara, K. Watanabe, H. Kinoshita, A. Yachi, Autoradiographic study on the site of uptake of the haptoglobin-hemoglobin complex, J. Reticuloendothel. Soc. 8 (2) (1970) 185–193.
[62] C.A. Schaer, G. Schoedon, A. Imhof, M.O. Kurrer, D.J. Schaer, Constitutive endocytosis of CD163 mediates hemoglobin-heme uptake and determines the noninflammatory and protective transcriptional response of macrophages to hemoglobin, Circ. Res. 99 (9) (2006) 943–950.
[63] L.E. Otterbein, R. Foresti, R. Motterlini, Heme Oxygenase-1 and carbon monoxide in the Heart: the Balancing Act between danger signaling and pro-survival, Circ. Res. 118 (12) (2016) 1940–1959.
[64] L.E. Otterbein, M.P. Soares, K. Yamashita, F.H. Bach, Heme oxygenase-1: unleashing the protective properties of heme, Trends Immunol. 24 (8) (2003) 449–455.
[65] R. Stocker, M.A. Perrella, Heme oxygenase-1: a novel drug target for atherosclerotic diseases? Circulation 114 (20) (2006) 2178–2189.
[66] I. Galea, S. Bandyopadhyay, D. Bulters, R. Humar, M. Hugelshofer, D.J. Schaer, et al., Haptoglobin treatment for aneurysmal subarachnoid hemorrhage: review and expert consensus on clinical translation, Stroke 54 (7) (2023) 1930–1942.
[67] A. Rubio-Navarro, J.M. Amaro Villalobos, J.S. Lindholt, I. Buendia, J. Egido, L. M. Blanco-Colio, et al., Hemoglobin induces monocyte recruitment and CD163-macrophage polarization in abdominal aortic aneurysm, Int. J. Cardiol. 201 (2015) 66–78.
[68] B. Hamann, A. Klimova, F. Klotz, F. Frank, C. Janichen, M. Kapalla, et al., Regulation of CD163 receptor in patients with abdominal aortic aneurysm and associations with antioxidant enzymes HO-1 and NQO1, Antioxidants 12 (4) (2023).
[69] A.V. Finn, M. Nakano, R. Polavarapu, V. Karmali, O. Saeed, X. Zhao, et al., Hemoglobin directs macrophage differentiation and prevents foam cell formation in human atherosclerotic plaques, J. Am. Coll. Cardiol. 59 (2) (2012) 166–177.
[70] A. Sakamoto, R. Kawakami, M. Mori, L. Guo, K.H. Paek, J.V. Mosquera, et al., CD163+ macrophages restrain vascular calcification, promoting the development of high-risk plaque, JCI Insight. 8 (5) (2023).
[71] C. Gutierrez-Munoz, N. Mendez-Barbero, P. Svendsen, C. Sastre, V. Fernandez-Laso, P. Quesada, et al., CD163 deficiency increases foam cell formation and plaque progression in atherosclerotic mice, FASEB J. 34 (11) (2020) 14960–14976.
[72] A. Sakamoto, A. Grogan, R. Kawakami, A. Finn, P. Shah, D. Nair, et al., Role of hemoglobin-stimulated macrophages and intraplaque hemorrhage in the development of vascular diseases, Arterioscler. Thromb. Vasc. Biol. 45 (7) (2025) 1021–1030.
[73] P. Li, M. Li, M.R. Lindberg, M.J. Kennett, N. Xiong, Y. Wang, PAD4 is essential for antibacterial innate immunity mediated by neutrophil extracellular traps, J. Exp. Med. 207 (9) (2010) 1853–1862.
[74] Z. Yuan, Y. Lu, J. Wei, J. Wu, J. Yang, Z. Cai, Abdominal aortic aneurysm: roles of inflammatory cells, Front. Immunol. 11 (2020) 609161.
[75] M. Salarian, M. Ghim, J. Toczek, J. Han, D. Weiss, B. Spronck, et al., Homeostatic, non-canonical role of macrophage elastase in vascular integrity, Circ. Res. 132 (4) (2023) 432–448.
[76] J.B. Michel, J.L. Martin-Ventura, J. Egido, N. Sakalihasan, V. Treska, J. Lindholt, et al., Novel aspects of the pathogenesis of aneurysms of the abdominal aorta in humans, Cardiovasc. Res. 90 (1) (2011) 18–27.

Graphical Abstract